Design of Piezoelectric Weigh-in Motion Systems Based on PZT Material Composite Structure

by

Gongyuan Liu

BS Mechanical Engineering, University of Pittsburgh, 2019

Submitted to the Graduate Faculty of the

Swanson School of Engineering in partial fulfillment

of the requirements for the degree of

Master of Science in Mechanical Engineering

University of Pittsburgh

2021

UNIVERSITY OF PITTSBURGH

SWANSON SCHOOL OF ENGINEERING

This thesis was presented

by

Gongyuan Liu

It was defended on

April 7, 2021

and approved by

Patrick Smolinski, Ph.D., Associate Professor, Department of Mechanical Engineering and Materials Science

William S. Slaughter, Ph.D., Associate Professor, Department of Mechanical Engineering and Material Science

Thesis Advisor: Qing-Ming Wang, Ph.D., Professor, Department of Mechanical Engineering and Materials Science

Design of Piezoelectric Weigh-in Motion Systems Based on PZT Material Composite Structure

Gongyuan Liu, MS

University of Pittsburgh, 2021

Weigh-in-Motion (WIM) is the process of measuring the dynamic tire forces while the vehicles are in motion and estimating the corresponding static loads of vehicles at rest. In this thesis, two piezoelectric weigh-in-motion systems that involve bending and compression mode structural design are developed. Lead Zirconate Titanate (PZT) ceramic plate is chosen as the sensing element of the sensor because of its large piezoelectric charge coefficient, moderate permittivity, and high coupling factor. The relations between output charge, voltage, and applied loads of each design were derived theoretically. A charge-amplifier circuit was designed to make the output signal readable. The performance of compression mode and bending mode structure were compared. In the experiment, the hand truck with different weights is used to roll over the sensors. The results show that the compression mode performs good linearity under different mass and speeds. The experimental sensitivity of the compression mode is very close to the theoretical value. For bending mode, the experimental output voltage is much smaller than the compression mode, and it is highly affected by the speed of the hand truck. The experimental sensitivity is more closed to the theoretical value when the speed is higher. Then, Fourier transform was used to get the frequency spectrum of the output signal. By observing the output signals, we found that its dominant frequency was related to the vehicle's speed, but the estimated speed is not accurate. A Bluetooth wireless transmission unit is also designed to realize the wireless monitoring of the vehicle weight.

Table of Contents

List of Tables

List of Figures

Preface

I would like to express my sincerest appreciation to my thesis advisor, Dr. Qing-Ming Wang, for all his encouragement, support, and guidance in this work and over the past two years of my M.S. study. I am very thankful to Dr. William Slaughter and Dr. Patrick Smolinski for their willingness to attend my thesis defense as my committee members.

Meanwhile, I would like to thank my colleagues Zihao Zhong, Saleh Alghamdi, Wenhao Huang, Ruixin Feng, Wenxiang Qian, and Weibo Gao for their help in my research.

Finally, I would like to express my deepest gratitude to my families, who are always supporting me and loving me in my life.

1.0 Introduction

This chapter will introduce the history of piezoelectricity and lead zirconate titanate (PZT), discuss the fundamentals of piezoelectric transducers according to published literature.

1.1 History

Piezoelectricity, which originates from the Greek language, means electricity due to pressure[1]. In 1880, Curie brothers firstly recognized the effect that electric charges would be generated when mechanical forces were applied to material like tourmaline, quartz, topaz, and Rochelle salt, which is referred to as direct piezoelectric effect[2]. In 1881, Gabriel Lippman derived inverse piezoelectric effect mathematically[3], which indicated that the piezoelectric materials also conversely have a geometric strain under an applied electric field. Then, Curie brothers proved its existence experimentally immediately.

During World War I, Langevin and his coworker developed sonar (ultrasonic submarine detector), which is the first practical application of piezoelectricity [4]. They glued a thin quartz crystal between two steel plates and detected the return of echo by a hydrophone. In 1921, Walter Guyton Cady invented the quartz crystal oscillator, which was used in all high-frequency radio transmitters. Nowadays, the quartz crystal oscillator works as a secondary standard for timing and frequency control[5]. The success of the sonar and crystal oscillator boosted the development of the application of piezoelectric devices.

Researchers discovered a new type of synthetic material called ferroelectrics during World War II[3]. This type of material such as Barium titanite provides much higher piezoelectric constant than natural materials such as quartz. Then, around 1952, Tokyo zirconate titanate was developed by Tokyo Institute of Technology[6], [7]. Now, PZT becomes one the most used piezo ceramics in industries due to its high electromechanical factor and relatively low manufacture costs.

1.2 Fundamentals of Sensors and Actuators

Sensors and actuators play an important role in our life and industries. This section aims to introduce what sensors and actuators are and how they work.

A sensor is a device that responds to a physical stimulus (such as heat, light, sound, pressure, magnetism, or a particular motion) and transmits a resulting impulse (as for measurement or operating a control)[8]. In our research, sensors convert mechanical quantities into electrical signals.

In contrast to sensors, actuators convert electrical signals like voltage into mechanical quantity like force and movement. From the system point of view, electrical signals serve as inputs, whereas mechanical represent outputs of actuators.

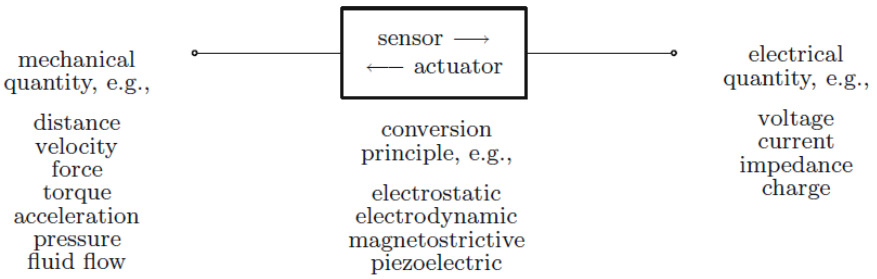

Figure 1.1: Conversion principles of sensors and actuators[1]

The conversion principles are shown in Figure 1.1. Since both sensors and actuators can convert energy from one form to another, they are also called transducers. Piezoelectric materials are widely used as the components of sensors and actuators due to their ability to convert electrical and mechanical energy mutually.

1.3 Fundamentals of Piezoelectricity

In this section, we will discuss the principle of the piezoelectric effect. The piezoelectric effect is understood as the linear interaction between mechanical quantity and electric quantity[1]. Materials with piezoelectricity are referred to as piezoelectric materials. Due to the applied mechanical load, the mechanical deformation of this material will cause a macroscopic change in the electrical polarization, which will generate charges on the surface of material. Using a suitable electrode covering material, we can measure the voltage or charge directly related to mechanical deformation. Inversely, the applied voltage can also cause the mechanical deformation of piezoelectric material, this phenomenon is called inverse piezoelectric effect.

To understand the piezoelectric effect in more detail, we need to understand the microscopic structure of piezoelectric material. Let us use quartz, a natural piezoelectric material, as an example. Quartz has a crystal structure that lacks a center of symmetry. Figure 1.2 (a) shows the structure of a unit cell of quartz crystal without external load. Silicon and oxygen ions form a regular hexagon structure, which means that the angles between those three electric dipole moments are all 120°. The centers of positive charges C_{Q+} and negative charges C_{Q-} are geometrically coincident. Hence, there is no charge generated on the surface of the crystal. Figure 2(b) and (c) show the deformation of the crystal structure while force is applied vertically and horizontally. After an external load is applied, the deformations cause the movements of centers of charges C_{Q+} and C_{Q-} which results in electric dipole moments. The dipole moment is characterized by the electric polarization, which is denoted as **P** in the figure. The magnitude of P increases with the distance between C_{Q+} and C_{Q-}. To compensate the electric polarization within the material, charges will be induced on the surface of the material.

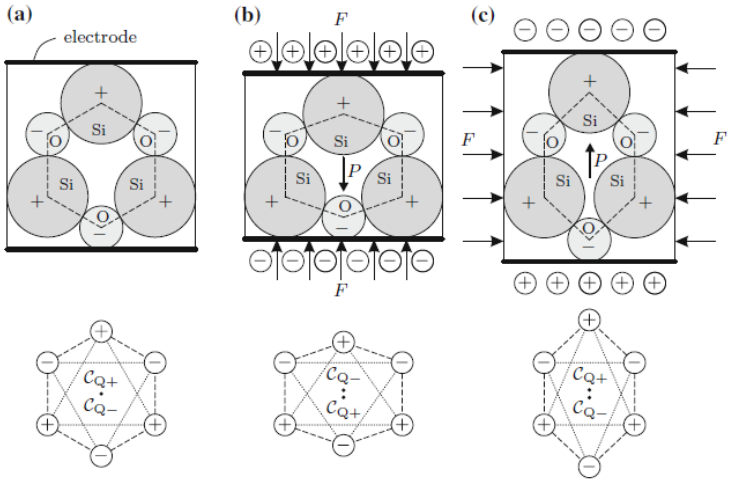

Figure 1.2:Molecular Model of Piezoelectric Effect of Quartz[1]

As we mentioned in Section 1.2, synthetic material such as barium titanate ($BaTiO_3$), lead titanate (PbTiO3), and lead zirconate titanate (PZT) ceramics provides better piezoelectric property than natural material, and they are widely used in industries. Below a critical temperature, Curie point, materials with perovskite crystal structure have a dipole moment. For example, in PZT (Figure 1.3, b), the material has a small dipole moment because the position of Zr^{4+} or Ti^{4+} cation is not centered. If the temperature is higher than Curie point, the element exhibits a simple cubic symmetry with no dipole moment (Figure 1.3, a).

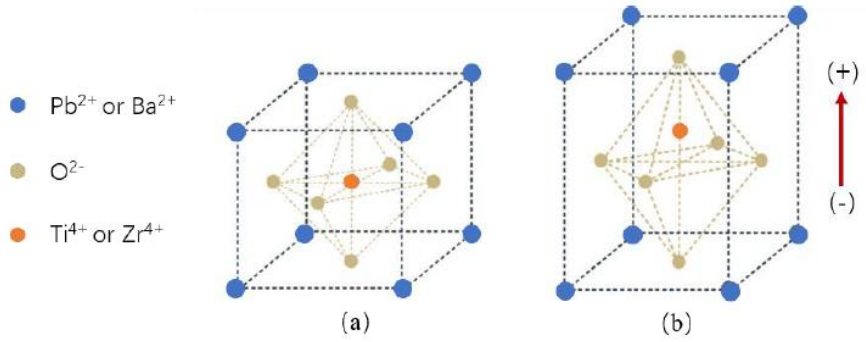

Figure 1.3: Crystal structure of a typical piezoelectric ceramic: (a) the case where temperatures are above the Curie point; (b) the case where temperatures are below the Curie point [9]

These materials are always manufactured by sintering the powders, and the powders form a dense polycrystalline structure. Therefore, the polarization direction of each unit cell is distributed randomly, which is shown in figure 1.4(a). The region of adjacent dipoles is called domain, and the net dipole moment of this region gives a net polarization of the domain. Since the direction of polarization among neighboring domains is random, the ceramic element shows no polarity in Figure1.4 (a). In order to get a piezoelectric material with an aligned direction of

polarization, we need to apply a strong DC electric field on the material along a certain direction at a temperature below the Curie point (Figure1.4 (b)). The process above is called poling. After poling process, the element will have a permanent polarization, which is called remanent polarization.

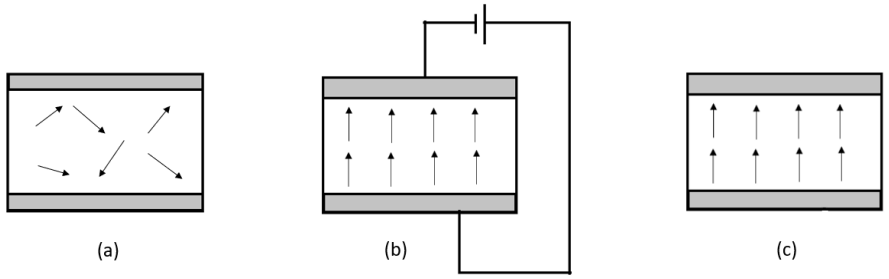

Figure 1.4: Polarizing Process: (a)unpoled ceramic; (b) poling with DC electric field; (c) polarized

Poling direction is a critical property for piezoelectric material since it determines the linear relations between input and output signal[10].

The linear relations of piezoelectricity are given by the equation called constitutive equations. To derive the constitutive equations, we need to linearize the energy equations,

$$dD_m = \varepsilon_{mn}^{T,\vartheta} dE_n + d_{mkl}^{\vartheta} dT_{kl} + \rho_m^T d\vartheta \tag{1-1}$$

$$dS_{ij} = d_{ijn}^{\vartheta} dE_n + s_{ijkl}^{E,\vartheta} dT_{kl} + \alpha_{ij}^E d\vartheta \tag{1-2}$$

where D is electric flux density, E is electric field intensity, T is mechanical stress, ϑ is

temperature. ε^T is the electric permittivity under constant mechanical stress, s is the elastic compliance constants, d is the piezoelectric strain constant, ρ is the pyroelectric coefficient, α is the thermal expansion coefficient.

Assume the isothermal condition ($d\vartheta$=0), Eqs. (1-1) and (1-2) could be simplified as,

$$dD_m = \varepsilon_{mn}^T dE_n + d_{mkl} dT_{kl} \tag{1-3}$$

$$dS_{ij} = d_{ijn} dE_n + s_{ijkl}^E dT_{kl} \tag{1-4}$$

Assume the initial condition, $D_m = E_n = S_{ij} = T_{kl} = 0$ at the initial state. By solving the differential equation, Eqns (1-3) and (1-4) will become,

$$D_m = \varepsilon_{mn}^T E_n + d_{mkl} T_{kl} \tag{1-5}$$

$$S_{ij} = d_{ijn} E_n + s_{ijkl}^E T_{kl}\,, \tag{1-6}$$

which represents the d-form (strain charge form) of the material law for linear piezoelectricity.

Due to symmetries within the tensors of rank 3 and rank 4 mechanical field, the number of independent components of s_{ijkl} and d_{mkl} in Eqn. (1-5) and (1-6) can be reduced significantly by Voigt notation[11]. Therefore, the equations can be written in matrix form as:

$$D = [\boldsymbol{\varepsilon^T}]E + [d]T$$
$$S = [\boldsymbol{d}]^T E + [\boldsymbol{s^E}]T \quad (1\text{-}7)$$

By rearranging the Equation (1.3.7), different form of constitutive equations can be yielded,

e-form:

$$D = [\boldsymbol{\varepsilon^S}]E + [\boldsymbol{e}]S$$
$$T = -[\mathbf{e}]^{\mathbf{T}}E + [\boldsymbol{c^E}]S \quad (1\text{-}8)$$

g-form:

$$E = [\boldsymbol{\beta^T}]D - [\boldsymbol{g}]T$$
$$S = [\boldsymbol{g}]^T D + [\boldsymbol{s^D}]T \quad (1\text{-}9)$$

h-form:

$$E = [\boldsymbol{\beta^S}]D - [\boldsymbol{h}]S$$
$$T = -[\boldsymbol{h}]^T D + [\boldsymbol{c^D}]S. \quad (1\text{-}10)$$

Where ε^S is the electric permittivity for constant mechanical strain, s is the elastic compliance constants, c is the elastic stiffness constant, e is the piezoelectric stress constant, g is the piezoelectric voltage constant, h is the piezoelectric charge constant, and β is the impermeability.

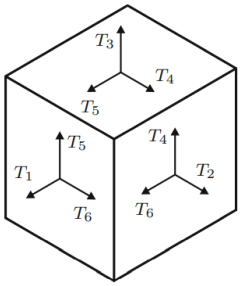

Figure 1.5: Voigt Notation

Figure 1.3.4 shows the common notation in constitutive for piezoelectricity with respect to Cartesian coordinate system xyz in three-dimensional space. Take d-form as an example, the vector for electric flux density **D** contains 3 components. The mechanical stress **T** and strain **S** vectors contains 6 independent components. The dimensions of piezoelectric coefficient tensor **[d]** and elastic compliance constant **[s^E]** are 3×6 and 6×6. Therefore, the d-form constitutive equation can be expanded as,

$$\begin{bmatrix} D_1 \\ D_2 \\ D_3 \end{bmatrix} = \begin{bmatrix} \varepsilon_{11}^T & \varepsilon_{12}^T & \varepsilon_{13}^T \\ \varepsilon_{21}^T & \varepsilon_{22}^T & \varepsilon_{23}^T \\ \varepsilon_{31}^T & \varepsilon_{32}^T & \varepsilon_{33}^T \end{bmatrix} \begin{bmatrix} E_1 \\ E_2 \\ E_3 \end{bmatrix} + \begin{bmatrix} d_{11} & d_{12} & d_{13} & d_{14} & d_{15} & d_{16} \\ d_{21} & d_{22} & d_{23} & d_{24} & d_{25} & d_{26} \\ d_{31} & d_{32} & d_{33} & d_{34} & d_{35} & d_{36} \end{bmatrix} \begin{bmatrix} T_1 \\ T_2 \\ T_3 \\ T_4 \\ T_5 \\ T_6 \end{bmatrix} \tag{1-11}$$

$$\begin{bmatrix} S_1 \\ S_2 \\ S_3 \\ S_4 \\ S_5 \\ S_6 \end{bmatrix} = \begin{bmatrix} d_{11} & d_{21} & d_{31} \\ d_{12} & d_{22} & d_{32} \\ d_{13} & d_{23} & d_{33} \\ d_{14} & d_{24} & d_{34} \\ d_{15} & d_{25} & d_{35} \\ d_{16} & d_{26} & d_{36} \end{bmatrix} \begin{bmatrix} E_1 \\ E_2 \\ E_3 \end{bmatrix} + \begin{bmatrix} s_{11}^E & s_{12}^E & s_{13}^E & s_{14}^E & s_{15}^E & s_{16}^E \\ s_{21}^E & s_{22}^E & s_{23}^E & s_{24}^E & s_{25}^E & s_{26}^E \\ s_{31}^E & s_{32}^E & s_{33}^E & s_{34}^E & s_{35}^E & s_{36}^E \\ s_{41}^E & s_{42}^E & s_{43}^E & s_{44}^E & s_{45}^E & s_{46}^E \\ s_{51}^E & s_{52}^E & s_{53}^E & s_{54}^E & s_{55}^E & s_{56}^E \\ s_{61}^E & s_{62}^E & s_{63}^E & s_{64}^E & s_{65}^E & s_{66}^E \end{bmatrix} \begin{bmatrix} T_1 \\ T_2 \\ T_3 \\ T_4 \\ T_5 \\ T_6 \end{bmatrix} \tag{1-12}$$

For 4-mm crystal class like PZT and $BaTiO_3$, there are further symmetries within the piezoelectric material. The constitutive equation could be simplified as,

$$\begin{bmatrix} D_1 \\ D_2 \\ D_3 \end{bmatrix} = \begin{bmatrix} \varepsilon_{11}^T & 0 & 0 \\ 0 & \varepsilon_{11}^T & 0 \\ 0 & 0 & \varepsilon_{33}^T \end{bmatrix} \begin{bmatrix} E_1 \\ E_2 \\ E_3 \end{bmatrix} + \begin{bmatrix} 0 & 0 & 0 & 0 & d_{15} & 0 \\ 0 & 0 & 0 & d_{15} & 0 & 0 \\ d_{31} & d_{31} & d_{33} & 0 & 0 & 0 \end{bmatrix} \begin{bmatrix} T_1 \\ T_2 \\ T_3 \\ T_4 \\ T_5 \\ T_6 \end{bmatrix} \tag{1-13}$$

$$\begin{bmatrix} S_1 \\ S_2 \\ S_3 \\ S_4 \\ S_5 \\ S_6 \end{bmatrix} = \begin{bmatrix} 0 & 0 & d_{31} \\ 0 & 0 & d_{31} \\ 0 & 0 & d_{33} \\ 0 & d_{15} & 0 \\ d_{15} & 0 & 0 \\ 0 & 0 & 0 \end{bmatrix} \begin{bmatrix} E_1 \\ E_2 \\ E_3 \end{bmatrix} + \begin{bmatrix} s_{11}^E & s_{12}^E & s_{13}^E & 0 & 0 & 0 \\ s_{12}^E & s_{22}^E & s_{13}^E & 0 & 0 & 0 \\ s_{13}^E & s_{13}^E & s_{33}^E & 0 & 0 & 0 \\ 0 & 0 & 0 & s_{44}^E & 0 & 0 \\ 0 & 0 & 0 & 0 & s_{55}^E & 0 \\ 0 & 0 & 0 & 0 & 0 & s_{66}^E \end{bmatrix} \begin{bmatrix} T_1 \\ T_2 \\ T_3 \\ T_4 \\ T_5 \\ T_6 \end{bmatrix} \tag{1-14}$$

The first equation relates to the linear relation for the direct piezoelectric effect and the second one for the inverse piezoelectric effect. For sensors, we mainly consider the direct piezoelectric effect, assume there is no applied electric field *E*, the equation (1-15) becomes,

$$\begin{bmatrix} D_1 \\ D_2 \\ D_3 \end{bmatrix} = \begin{bmatrix} 0 & 0 & 0 & 0 & d_{15} & 0 \\ 0 & 0 & 0 & d_{15} & 0 & 0 \\ d_{31} & d_{31} & d_{33} & 0 & 0 & 0 \end{bmatrix} \begin{bmatrix} T_1 \\ T_2 \\ T_3 \\ T_4 \\ T_5 \\ T_6 \end{bmatrix} \tag{1-15}$$

Then, the generated charge can be determined by calculating the integral of D_i with respect to the area of electrode, and the generated voltage V can be calculated by,

$$q = \int D_i \, dA_i = d_{ij} F_j. \tag{1-16}$$

$$V = \frac{q}{C_p}. \tag{1-17}$$

where C_p is equivalent capacitance of piezoelectric material.

The equation for calculating the equivalent capacitance of piezoelectric material with electrodes on the surfaces perpendicular to the 3-axis is,

$$C_p = \frac{lw\varepsilon_{33}}{t}. \tag{1-18}$$

Due to the symmetries within the 4mm class ceramic, the piezoelectric coefficient matrix is reduced to 3 distinct piezoelectric constant d_{33}, d_{31}, and d_{15}, these coefficients are closely related to the sensitivity of a piezoelectric sensor. Generally, d_{15} is five times larger than d_{33}, and d_{33} is twice as large as d_{31}. The piezoelectric elements are divided into 3 different modes according to the force-charge relations, which is shown in Figure 1.6. As we can see from Figure 1.6(a), d_{15} mode implies that the shear stress is applied along the 5-axis, and the charge is generated on the electrodes on the surfaces perpendicular to 1-axis. The d_{33} mode and d_{31} mode imply that the charge

generation happens on the electrodes on the surfaces perpendicular to 3-axis with force along 1-axis (d_{31} mode) and 3-axis (d_{33} mode).

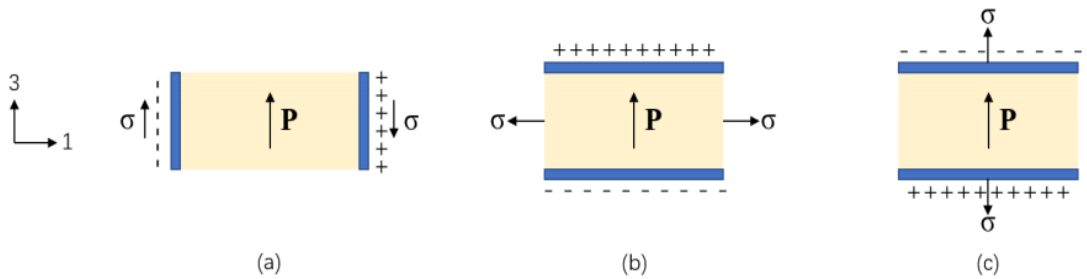

Figure 1.6: Force- charge relationship of piezoelectric element (a)d15 (b)d31 (c)d33

According to figure 6 and equation 6 and 7, the induced voltage V for d33 and d31 mode can be derived,

$$V_{33} = \frac{d_{33} F_3 t}{\varepsilon_{33} l w} \tag{1-19}$$

$$V_{31} = \frac{d_{31} F_1 t}{\varepsilon_{33} l w} \tag{1-20}$$

where *l*, *w*, and *t* are the length, width, and thickness of a piezoelectric material. According to these equations, we can find that the output voltage is linearly related to the applied force/mechanical stress. Hence, sensors such as accelerometer, pressure sensor, load cell are designed through these linear relations.

2.0 Background

2.1 Weigh in Motion

The static weights of vehicles play important roles in pavement analysis and design. Generally, these weights can be measured by pulling the vehicles to the weigh stations while vehicles are rest[12]. However, weighing stations on highways are also accompanied by several disadvantages including being dangerous, time-consuming, and expensive. Therefore, weighing the vehicles in motion has become a challenge for engineers.

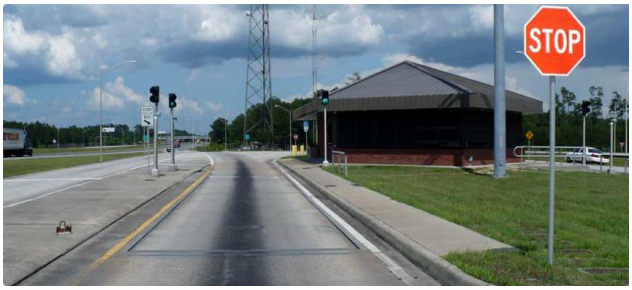

Figure 2.1：Weigh Station [13]

Weigh-in-Motion (WIM) is the process of measuring the dynamic tire forces while the vehicles are in motion and estimating the corresponding static loads of vehicles at rest. The WIM systems can estimate the gross weight of a vehicle as well as the portion of this weight, which is carried by the tires of each axle/axle group on the vehicle[14], [15]. WIM systems provide a safer and more time-saving and economical solution for weighing the vehicle on highways.

WIM systems usually place the sensors under the road lane to weigh the vehicles. The common weighing devices include piezoelectric sensors, bending plates, load cells. These systems undergo severe wear and tear, which results in a short lifespan [12]. Moreover, the smoothness of the pavements and the speeds of the vehicles have a significant influence on the result. In order to get more accurate results, novel sensors including optic fiber weighing sensors[16], Capacitive flexible weighing sensors[17], and multiple sensor WIM are developed.

The sensing elements of bending plates and load cells are strain gauges. The advantage of the strain gauge is its low price. However, its dynamic response to the pavement deflection is slow which makes its output more susceptible to the speed of vehicles. For a piezoelectric sensor, since piezoelectric materials are applied as sensing elements, it has very high sensitivity and quick dynamic response. Wenbin Zhang et al. conducted a comparison of time response for a two-axle vehicle between the strain gauge and the piezoelectric WIM system and the results are shown in Figure 2.2 [12]. As we can see from Figure 2.2 (a), it is obvious that the response of the strain gauge is so slow that the first waveform had not finished when the second wave came. This phenomenon results in inaccuracy when weighing high-speed vehicles. However, piezoelectric sensors (Figure 2.2 (b)) with fast response are capable of measuring two complete waveforms. This comparison shows that piezoelectric sensors will provide better accuracy in dynamic force measurement.

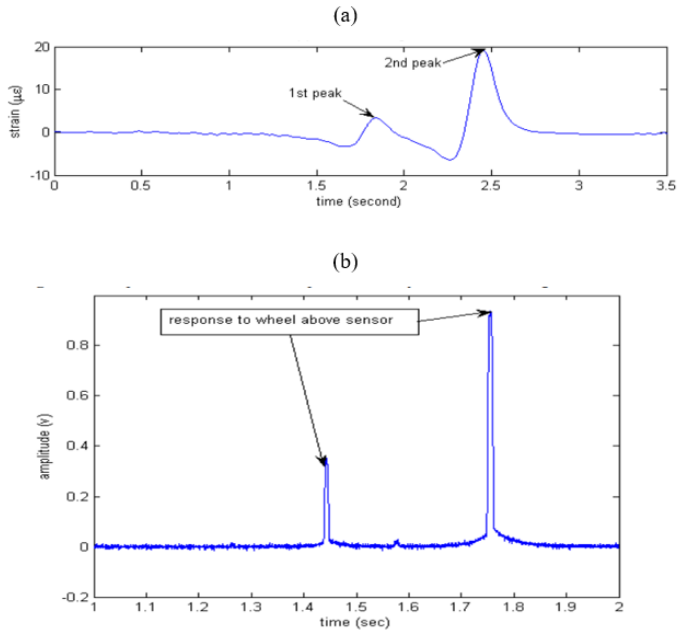

Figure 2.2：Comparison of the dynamic response of (a)strain gauge, (b)piezoelectric sensor

2.2 General Structure of Piezoelectric Sensor

Three basic structural designs are commonly used in manufacturing piezoelectric sensors: flexural, compression, and shear[18], as shown in Figure 2.3. Each structural design corresponds to a force-charge relationship mentioned in the previous section.

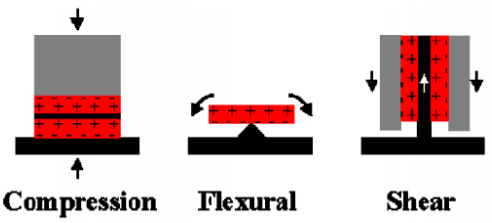

Figure 2.3：Structural Designs of piezoelectric sensors[18]

For flexural design which applies the d_{31} mode, the piezoelectric element is bent, and the bending stress generates the voltage along 1-axis. Since the thickness of the piezoelectric element is usually small, the moment of inertia about the 1-axis will also be tiny. According to the equation of bending stress,

$$\sigma = \frac{Mc}{I} \tag{2-1}$$

where M is the bending moment, c is the distance to the neutral axis, and I is the moment of inertia.

The small moment of inertia brings large bending stress under a specific moment. Due to the linear relationships, the output voltage will also be very high. Therefore, sensors with flexural designs have very high sensitivities. However, this design is limited by the low resonance frequency of the sensor structure, and the frequency range is much lower than compression and shear mode sensors. Also, the flexural design is the least durable of these three structures.

The compression design, which applies the d_{33} mode of the piezoelectric element, is the most straightforward design. Since the vibration mode of the piezoelectric sensing element is thickness vibration, the resonance frequency high, which gives this structure a wider frequency range and better durability. The sensor sensitivity is consistent at different frequency[19]. However, the disadvantage of this design is that the output signal is affected by thermal transients due to the pyroelectricity inherent to ferroelectric materials. Therefore, sensors with this design always use thick base and thick-walled structures to compensate base strain and the thermal transient sensitivities[18].

The shear design applies d_{15} mode, which is always used in accelerometers. This structure does not produce false signal as the other designs because this structure measures the signal along

1-axis, and according to Equation (1-15), only the stress along 5-axis determines the magnitude of the output signal. Also, this design has a low thermal transient sensitivity since the pyroelectricity generates charges along polarization direction (3-axis).

2.3 Design of Piezoelectric Sensor for WIM Systems

2.3.1 Compression mode dynamic force sensor

Dynamic force sensor is the most straightforward method to weigh the vehicle in motion. Piezoelectric materials are widely used as the sensing elements due to the fast response and high sensitivity. The compression mode is applied as the structural design. The sensor is designed to weigh vehicles which means that the forces exerted on the PZT sensing element are high enough to generate a strong signal. Therefore, compression mode is suitable for this application even though its sensitivity is relatively lower than the other modes.

As shown in Figure 2.4, two square PZT plates are bonded under a thick steel bar, and the widths of the steel bar and the PZT films are the same. The steel bar needs to be wide and long enough to ensure the axle loads of the testing dolly can be applied to the sensing element completely. The bottom surfaces of PZT films are bonded on the firm ground, which reduces the impact of vibration of the steel bar to the output signal. The PZT films are placed under the wheels of vehicles; once a vehicle drives over the steel bar, its wheels will compress the PZT films, based on the linear relationship along d_{33} direction, the amplitude of the output signal should be proportional with the weight of the vehicle.

Figure 2.4: Sketch of Compression Mode Design

2.3.1.1 Static Analysis of Compression Mode Sensor

Sensor sensitivity refers to the ratio between the output voltages and the input parameters. For the weigh-in-motion system, the input parameter is the weights of the vehicles. Therefore, the sensitivity of the WIM system can be calculated by,

$$Sensitivity = \frac{V_{out}}{F_{vehicle}}. \tag{2-2}$$

For compression mode sensors, loads of the vehicles are applied to the sensing element directly and completely. Hence, the output voltage can be calculated easily by applying the d_{33} mode linear relationship,

$$V_{out} = \frac{d_{33} F_{vehicle} t}{\varepsilon_{33} l w}. \tag{2-3}$$

Where *l*, *w*, and *t* are the length, width, and thickness of the PZT plate in this design. Then, according to equation 2.3 since the equation has shown us the relationship between output signal V_{out} and input parameter $F_{vehicle}$. By rearranging the equation, the theoretical sensitivity can be yielded,

$$Sensitivity = \frac{V_{out}}{F_{vehicle}} = \frac{d_{33}t}{\varepsilon_{33}lw}. \quad (2\text{-}4)$$

2.3.2 Bending Mode Design

When the vehicle's wheels roll over the sensor, we can consider this input signal as a pulse wave. Therefore, the structural design of pressure sensors is referenced in this part. Piezoelectric sensors apply d_{31} structure, which means that the sensing elements respond to the bending deflection of the surface where it is attached. The common structure of the unimorph piezoelectric sensor is shown in figure 2.5. The boundary of the substrate is clamped, and it will be deflected when uniform pressure is applied. Then, the piezoelectric layer will generate charge via d_{31} mode. Supposing the deflection is much smaller than the thickness of the sensor plate, based on the beam theory and piezoelectricity, the output signal of PZT film should be proportional to the amplitude of applied pressure.

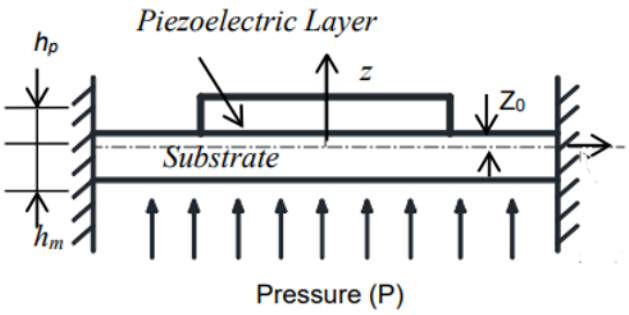

Figure 2.5: Unimorph Piezoelectric Pressure Sensor [20]

The bending mode WIM system is designed based on existing unimorph piezoelectric pressure sensor. As shown in Figure 2.6, since the wheels will roll over the top of the sensor, two sensing elements will be placed under a steel beam. The beam will be fixed supported at two ends.

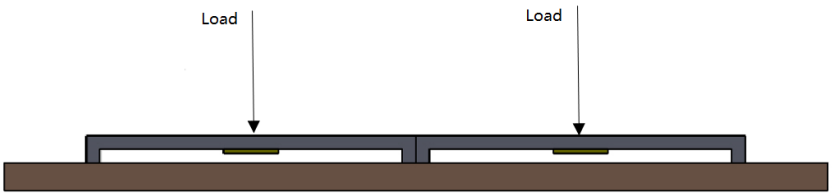

Figure 2.6: Bending Mode WIM system

2.3.2.1 Sandwiched Composite Structure

The PZT plates with a thickness of 1/80" are used in this study are also very fragile due to their small thickness. The Young's modulus of PZT ceramic is usually about 70 GPa[21]. However, bending/flexural mode sensors require relatively high flexibility of the sensing element.

In order to achieve the requirement, a thin insulating polymer film is used to cover the piezoelectric layer, and this structure is named as a sandwiched composite structure, which is shown in figure 2.7. With the support of the polymer layers, the sensing element has better flexibility and durability to bear the bending deflection of the steel beam.

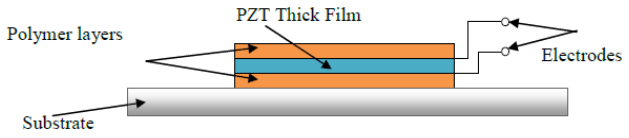

Figure 2.7: Sandwiched Composite Structure

2.3.2.2 Static Analysis of Bending Mode WIM System

In this case, the sensor is considered as a beam with two fixed ends, and the load of a wheel can be considered as a distributed load. The thickness of the beam is chosen as 0.5 inches, and the thickness of the PZT plate is 0.03 inches. Therefore, the thickness and the bending stiffness of the PZT layer can be neglected, which means that the deflection of the PZT layer is the same as the beams[22].

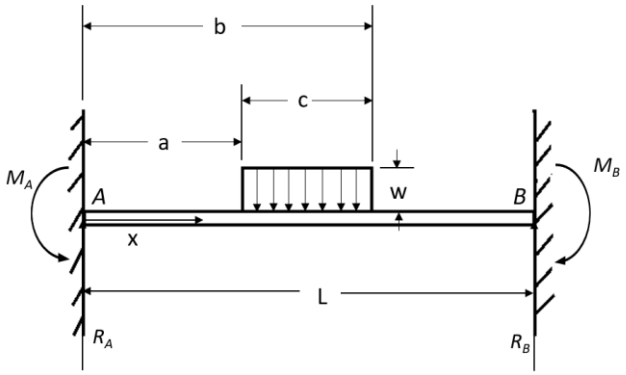

Figure 2.8: Free Body Diagram of the Sensor

Figure 2.8 shows the free body diagram of the sensor; since the uniform load w is applied at the middle of the beam, the reactions point A and B is,

$$R_A = R_B = \frac{wc}{2}. \tag{2-5}$$

$$M_A = -\frac{wc}{24L}\left(-\frac{6bc^2}{L} + \frac{3c^3}{L} + 4c^2 - 3L^2\right). \tag{2-6}$$

Then the bending moment equation at load-applied segment can be yielded,

$$M(x) = -M_A + R_A x - \frac{w}{2}(x-a)^2, \;\; a < x < b \tag{2-7}$$

By energy method, the deflection can be yielded,

$$y(x) = \frac{1}{6EI}[-3M_A x^2 + R_A x^3 - \frac{w}{4}(x-a)^4], \quad a < x < b \tag{2-8}$$

Using Euler-Bernoulli theory, the strain-displacement relation can be expressed as,

$$S(x,z) = -z\frac{\partial^2 y(x)}{\partial x^2} \tag{2-9}$$

According to the constitutive equation of piezoelectricity, the stress of sensing element is given by,

$$T_1 = -z\frac{\partial^2 y(x)}{s_{11}^E\, \partial x^2} - \frac{d_{31}E_3(x,z)}{s_{11}^E} \tag{2-10}$$

Since no electric field applied, the equation can be simplified as,

$$T_1 = -z\frac{\partial^2 y(x)}{s_{11}^E\,\partial x^2}. \tag{2-11}$$

Then, the polarization along the length of electrodes is obtained by integrating the constative equation through the thickness of the PZT layer,

$$D_3 = -\frac{d_{31}t}{s_{11}^E}\,\frac{\partial^2 y(x)}{\partial x^2} \tag{2-12}$$

Ideally, the distributed load is applied directly above the PZT element, and their widths are equal. The total charge output is given by integrating the polarization along the surface of the electrodes,

$$Q_3 = -\frac{d_{31}t}{s_{11}^E}\iint \frac{\partial^2 y(x)}{\partial x^2}\,dydx = -\frac{d_{31}tw}{s_{11}^E}\left[\frac{\partial y(x)}{\partial x}\right]_a^b \tag{2-13}$$

Then the output voltage will be

$$V_0 = -\frac{d_{31}t^2}{s_{11}^E\,\varepsilon_{33}c}\left[\frac{\partial y(x)}{\partial x}\right]_a^b \tag{2-14}$$

Then the sensor sensitivity is given by,

$$Sensitivity = -\frac{d_{31}t^2}{s_{11}^E\,\varepsilon_{33}w(x)c^2}\left[\frac{\partial y(x)}{\partial x}\right]_a^b \tag{2-15}$$

2.4 Research Objective

This research aims to construct two piezoelectric weigh-in-motion systems and discuss the dynamic response of the sensors in the frequency domain. In detail, most weigh-in-motion systems on the market focus on only the weights of vehicles. However, the dynamic response of a sensor is a waveform which means that it is also possible for WIM systems to acquire the speed of vehicles by analyzing the dynamic response of the sensor. Accordingly, the objectives of this thesis could be summarized as follows:

2.4.1 Design, fabrication, and calibration of PZT Weigh-in-Motion (WIM) systems in compression and bending modes.

This study applies the appropriate properties of PZT such as fast response, high sensitivity, and low cost to design and fabricate the weigh-in-motion systems in compression and bending mode. Signal conditioning circuits are designed according to the equivalent RC circuit for the PZT sensors, and the effective frequency ranges of the sensors are determined according to the dynamic response analysis. Next, install the WIM systems and push a dolly over the sensors to collect the time response data. Lastly, the time responses of these two sensors will be compared.

2.4.2 Analysis of output signal in frequency domain

Fast Fourier transform (FFT) is hired to convert the output signal from time domain to frequency domain. Then, knowing the fundamental frequency and the size of the sensor, the speeds of the hand truck can be estimated.

3.0 Equivalent Circuit of Piezoelectric sensors

The piezoelectric sensor usually consists of electrodes and a piezoelectric plate. Sensors need to be connected to the circuit to work. In this section, we will model an equivalent circuit which has the same property as the piezoelectric material. The equivalent circuit can make the analysis of circuit more accessible.

Piezoelectric materials generate electric charges in response to mechanical stress. Since there is no "charge source" in the standard circuit diagram, we can model the piezoelectric material as a current source because the current represents the rate of charge generation.

$$I = \frac{dQ}{dt} \tag{3-1}$$

Then, there are two electrodes coated on the upper and bottom surfaces of piezoelectric plates to introduce the charges into the output circuit. As we can see from the side view of the piezoelectric plate in Figure 3.1, two electrodes and the piezoelectric material form a capacitor. Hence, we can model the system as a current source connected to a capacitor, as shown in Figure 3.2.

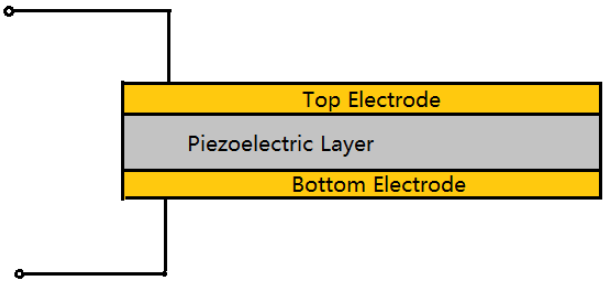

Figure 3.1：Side View of a Piezoelectric Plate

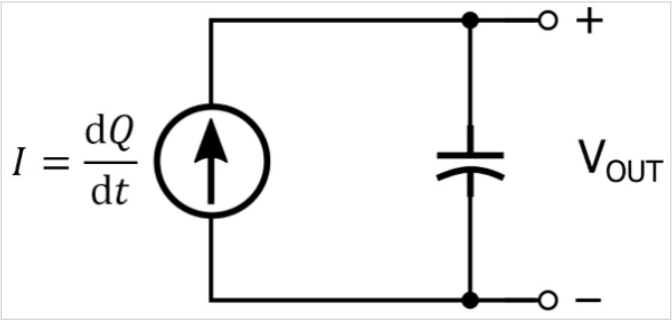

Figure 3.2 Equivalent Circuit of the Piezoelectric Plate

The output voltage of the equivalent circuit can be calculated by applying the current-voltage relation of the capacitor,

$$V = \frac{1}{C}\int \frac{dQ}{dt}dt \tag{3-2}$$

By calculating the integration, we can get the macroscopic expression of the relationship between voltage and charge of piezoelectric material[23],

$$V = \frac{Q}{C}. \tag{3-3}$$

As Equation 3.3 shown, the capacitance of the piezoelectric sample can be measured easily by a multimeter, and the theoretical value of generated charges can be calculated by Equation (1-16). Hence, the theoretical value of voltage generated under a specific load can be calculated easily.

Finally, although piezoelectric materials generate charges in response to mechanical stress, the charges do not stay forever. Therefore, to model this property, we can model this behavior by adding a parallel resistor to the equivalent circuit. The final sketch of the equivalent circuit is shown in Figure 3.3.

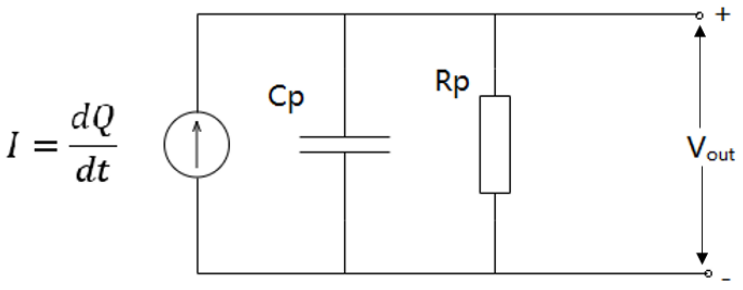

Figure 3.3: Final Sketch of Equivalent Circuit

For a piezoelectric material sample with a thickness of h, resistivity of ρ, and permittivity of ε. The resistance and capacitance of the sample can be written as,

$$R_p = \frac{\rho h}{A} \tag{3-4}$$

$$C_p = \frac{\varepsilon A}{h} \tag{3-5}$$

Therefore, the time constant which means that the time constant is only related to the property of the piezoelectric material is given by[23],

$$\tau_p = R_p C_p = \rho\varepsilon \tag{3-6}$$

3.1 Dynamic Response Analysis

In the case of mechanical vibration, the behavior of the piezoelectric sensor can be modeled as a simple mass-damper-spring structure, which is shown in Figure 3.4. Suppose a sinusoidal force $F(t) = Fsin\omega t$ is applied to the piezoelectric sensor, the equation of motion could be written as,

$$F(t) = mz\ddot{(t)} + cz\dot{(t)} + kz(t) \tag{3-7}$$

m…the effective mass

c…the damping coefficient

k…the effective spring constant

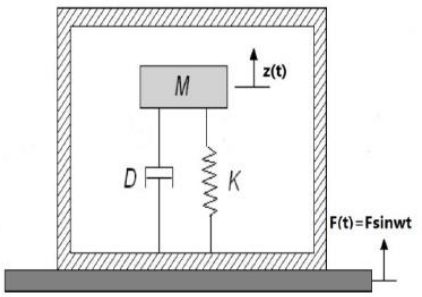

Figure 3.4: Mass-Sping-damper system

Then, take Laplace transform of both sides of the equation, the equation (3.7) becomes,

$$F(s) = ms^2Z(s) + csZ(s) + kZ(s) \tag{3-8}$$

Since we want a relationship between the output signal and natural frequency, substitute $s = j\omega$, natural frequency $\omega_n = \sqrt{\frac{k}{m}}$, and damping ratio $\zeta = \frac{d}{2\sqrt{km}}$, then the transfer equation could be yield,

$$\frac{Z(s)}{F(s)} = \frac{1}{k}\frac{\omega_n^2}{s^2 + 2\zeta\omega_n s + \omega_n^2} \tag{3-9}$$

As for electrical analysis, the equivalent circuit of piezoelectric sensors is discussed in the previous section, which is a parallel circuit composed of a current source, a resistance R_p, and a capacitance C_p. Applying Kirchhoff's current law, we can get the governing equation of the equivalent circuit,

$$\frac{dQ}{dt} = C_p\frac{dV}{dt} + \frac{V}{R_p} \tag{3-10}$$

Then, applying Laplace transform, we can get the transfer function,

$$\frac{V(s)}{Q(s)} = \frac{R_p s}{R_p C_p s + 1} \tag{3-11}$$

Then, substitute time constant $\tau = R_p C_p$. The time constant τ is the parameter to characterize the response to a step input of a first order, linear-time invariant system [24]. For a RC circuit, the time constant means the time required to charge the capacitor from zero to 63.2% of input DC voltage through a resistor or discharge 36.8% of initial voltage through a resistor.

$$\frac{V(s)}{Q(s)} = \frac{1}{C_p}\frac{\tau s}{\tau s + 1} \tag{3-12}$$

Since the value of generated charges Q is linearly related to the applied load F, and the strain and stress is also linearly related in the elastic deformation range, we can define a value K_q as the generated charge per displacement, $Q(t) = K_q Z(t)$.

Then the transfer function becomes:

$$\frac{V(s)}{Z(s)} = \frac{K_q}{C_p}\frac{\tau s}{\tau s + 1} \tag{3-13}$$

Combine Equations (3.9) and (3.13), we could finally get the transfer function for the piezoelectric sensor.

$$\frac{V(s)}{F(s)} = \frac{K_q}{kC_p}\frac{\omega_n^2}{s^2 + 2\zeta\omega_n s + \omega_n^2}\frac{\tau s}{\tau s + 1} \tag{3-14}$$

The sensitivity curve of piezoelectric sensor in frequency domain is shown in Figure 3.5. As we can see, the flat segment of the curve is called the usable region. It means that the output signal of the piezoelectric sensor is linear and frequency independent in this region, which means that the sensitivity of the sensor remains constant. The lower limit for the usable region depends on the value of equivalent resistance and capacitance: $f_{LL} = R_p C_p$. Since the equivalent circuit is

a RC circuit, input frequency should be high enough in order to get a stable and strong output signal. If the input frequency is too low, the RC circuit will discharge before the input signal(load/pressure) end, which severely influence the accuracy of the sensor. The upper limit frequency f_{UL} is the resonance frequency of sensor. The resonance frequency is determined by the mechanical structure and material property of the piezoelectric sensor.

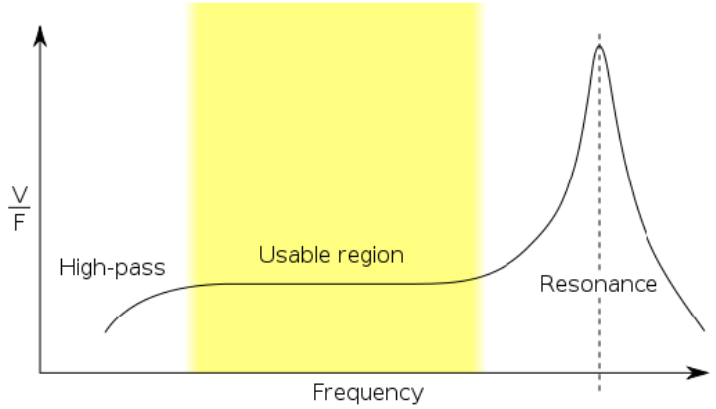

Figure 3.5: Frequency Response of the Piezoelectric Sensor System[25]

3.2 Design of Interface Circuit

An interface circuit is a signal conditioning circuit used to bring signal from the sensor up to the format that is compatible with the load device. For a piezoelectric device, charge is produced in response to applied mechanical stress. However, the piezoelectric coefficient d_{33} is usually about 400-600 pC/N. Since the amount of the generated charge is minimal, a charge amplifier is needed to convert the induced charge to a usable voltage for oscilloscope.

Another reason why the charge amplifier is needed is that the impedance of the piezoelectric sensor is enormous. The impedance of the piezoelectric sensor is usually higher than 1MΩ. However, the maximum input impedance of the Keysight 4024x Series oscilloscope is 1MΩ. The oscilloscope cannot measure a high impedance unit effectively since the assumption of measuring open circuit voltage does not hold in this scenario. When the sensor is connected to the circuit, the impedance will be greatly reduced, so the oscilloscope can read the output of the sensor accurately.

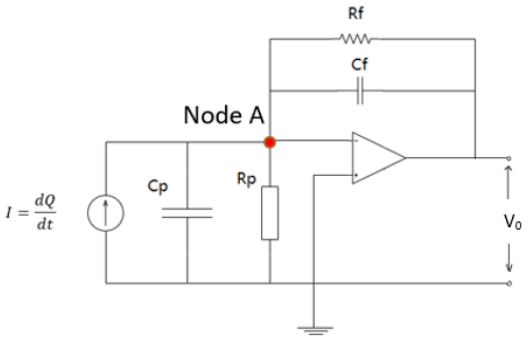

Figure 3.6: Sketch of Charge Amplifier

Apply Kirchhoff current law at node A in Figure 3.6, we can get the differential equation at node A,

$$\dot{q} + C_P \frac{dv_0}{A_0 dt} + C_c \frac{dv_0}{A_0 dt} + C_f \left(\frac{dv_0}{dt} + \frac{dv_0}{A_0 dt} \right) + \frac{v_0 + v_0/A_0}{R_f} = 0 \qquad (3\text{-}15)$$

where the term A_0 is the gain of the op-amp.

As mentioned at the beginning of this section, since the output signal of the sensor is extremely small, to get a usable signal, an enormous gain A_0 is needed. The value of A_0 is usually from 10^5 to 10^9.

Therefore, the equation 2.1 could be simplified as,

$$R_f C_f \frac{dv_0}{dt} + v_0 = -R_f \frac{dq}{dt} \ . \tag{3-16}$$

Applying Laplace transform on both side of the equation yields,

$$R_f C_f s V_0(s) + V_0(s) = -R_f Q(s). \tag{3-17}$$

Rearrange the equation, we can get the transfer function of the circuit,

$$\frac{V_0(s)}{Q(s)} = -R_f \frac{s}{R_f C_f s + 1}. \tag{3-18}$$

Substitute $s = j\omega$, we can get the transfer equation in the frequency domain,

$$\frac{V_0(j\omega)}{Q(j\omega)} = -\frac{R_f j\omega}{R_f C_f j\omega + 1} \ . \tag{3-19}$$

The frequency response of the sensor is shown in Figure 3.7. According to the figure, we can find that the circuit acts as a high-pass filter.

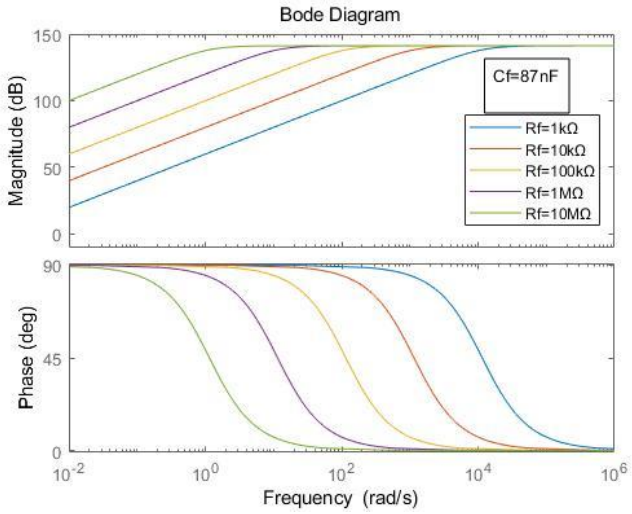

Figure 3.7: Bode Diagram of Charge Amplifier

According to the Equation (3-19), when the input frequency is 0, the output will be zero. At high frequency,

$$\frac{V_0(j\omega)}{Q(j\omega)} = -\frac{1}{C_f} \ . \tag{3-20}$$

This value is called calibration constant for the device.

For the charge amplifier shown in Figure 3.6, the time constant could be calculated by equation:

$$\tau_c = R_f C_f \ . \tag{3-21}$$

Next, we apply this result to the Equation 2.5, the transfer function can be written as,

$$G(j\omega) = \frac{\tau_c j\omega}{\tau_c j\omega + 1} \tag{3-22}$$

Then, calculate the magnitude of the transfer function,

$$M = \frac{\tau_c \omega}{\sqrt{\tau_c^2 \omega^2 + 1}} \ . \tag{3-23}$$

The measurement accuracy is defined as the closeness of magnitude M to 1. When the frequency approaches infinity, the magnitude M=1, which means that there is no sensor error. Suppose that we want the accuracy to be better than a value M_0, then the equation 2.9 could be written as,

$$\frac{\tau_c \omega}{\sqrt{\tau_c^2 \omega^2 + 1}} > M_0 \ . \tag{3-24}$$

Then, rearrange the equation, we can obtain the relationship between time constant τ_c and input frequency ω,

$$\tau_c > \frac{M_0}{\omega \sqrt{1 - M_0^2}} \ . \tag{3-25}$$

Hence, a specific lower limit of the input frequency under a specific level of accuracy can be achieved by changing the value of time constant.

Also, the transfer function is changed as the piezoelectric sensor connected to the charge amplifier. Therefore, the transfer function for the whole dynamic system will become,

$$\frac{V(s)}{F(s)} = -\frac{1}{C_f} \frac{\omega_n^2}{s^2 + 2\zeta\omega_n s + \omega_n^2} \cdot \frac{\tau_c s}{\tau_c s + 1} \tag{3-26}$$

Hence, the values of R_f and C_f determine the discharge time constant, which means that the low limit of the linear range could be changed by changing the values of R_f and C_f.

3.3 Fabrication Process of Sandwich Structure Sensor

This research applies PZT films with the sizes of 2’’x 2" x 0.125" as the sensing elements. Following processes are conducted to fabricate it to sandwich structure sensor:

a) First, model YE2730 d_{33} meter is used to measure the d_{33} coefficients of samples. As shown in Figure 3.8, PZT plates are clamped by the shaker. When the shaker starts working, the generated charges will be measured.

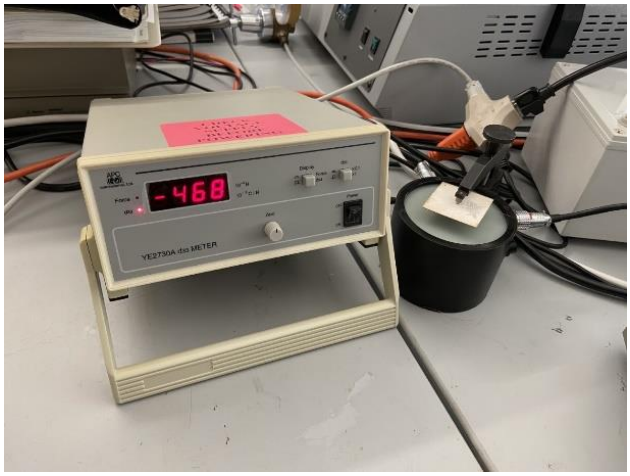

Figure 3.8: d33 Meter

b) Secondly, use silver epoxy and conductive tape to connect the wires to electrodes. Then, trim the Polyimide films (DuPont Kapton HN) with 75μm thickness as a square shape, clean up the surface of both PZT films and Polyimide films. After that, uniformly spin coat the epoxy (Eccobond 45 Clear, Ellsworth Adhesives, Germantown, WI) onto one side of Polyimide film,

then place the PZT film on the top of it. Then, cover the PZT film with another Polyimide film to form the sandwich structure.

c) Finally, bond the sandwiched sensor on the steel beam as the designs in Figure 3.9(a) and (b) by epoxy. The end product is shown in Figure 3.9(a) and (b)

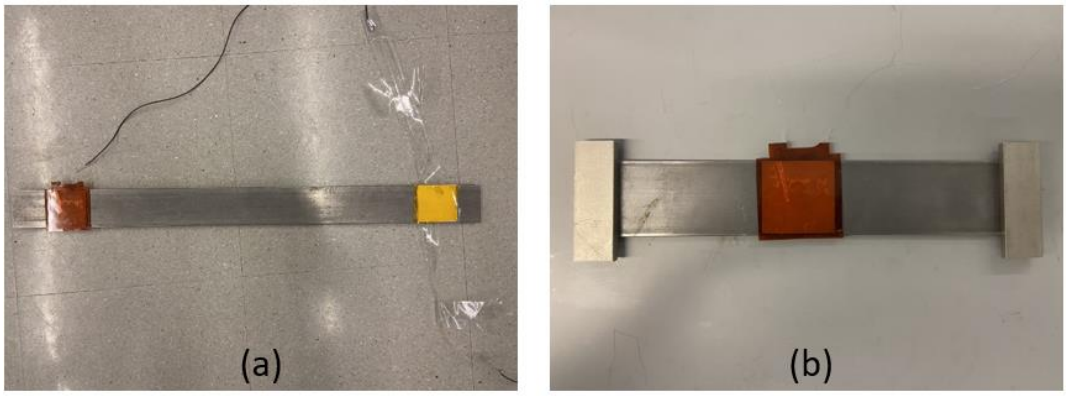

Figure 3.9: (a) Compression Mode (b) Bending Mode

In order to measure the equivalent resistance and capacitance for the PZT samples, the Agilent 4294A precision impedance analyzer is used. The impedance analyzer displays the frequency response of parallel resistance, parallel capacitance, impedance, and phase, shown in Figure 3.10 to Figure 3.13. The other important parameters of the sensor samples are listed in Table 3.1.

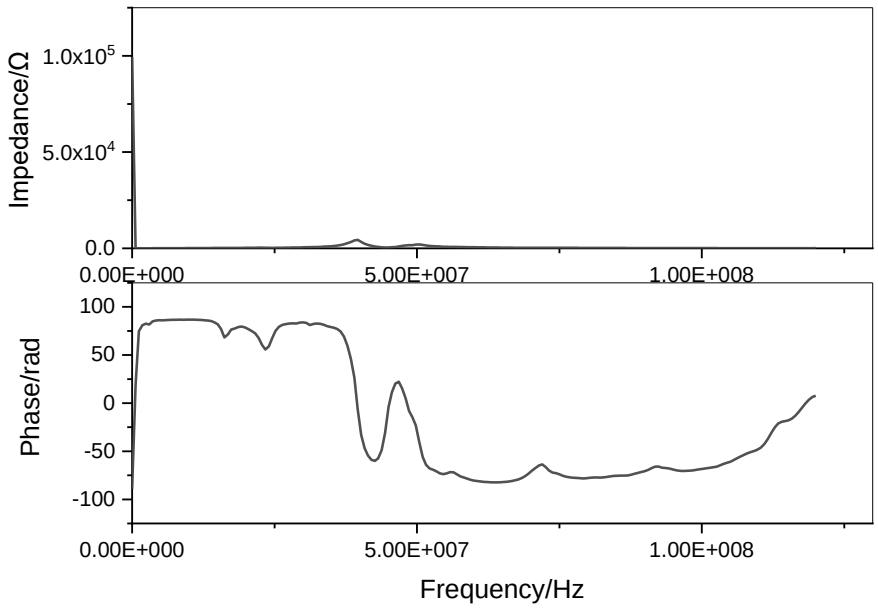

Figure 3.10: Frequency Response of Impedance of Compression Mode Sample

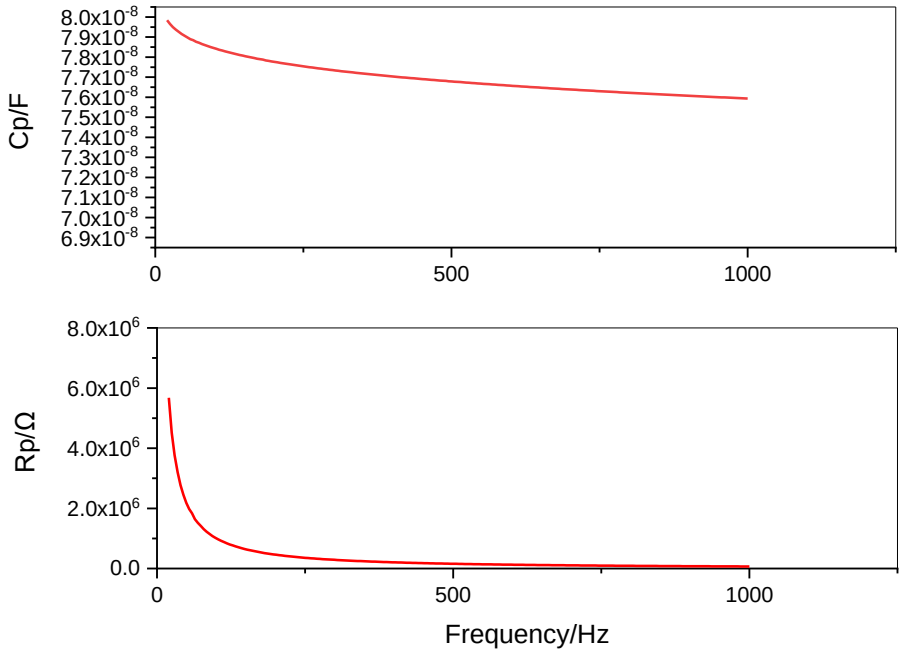

Figure 3.11: Equivalent Capacitance and Resistance of Compression Mode Sample

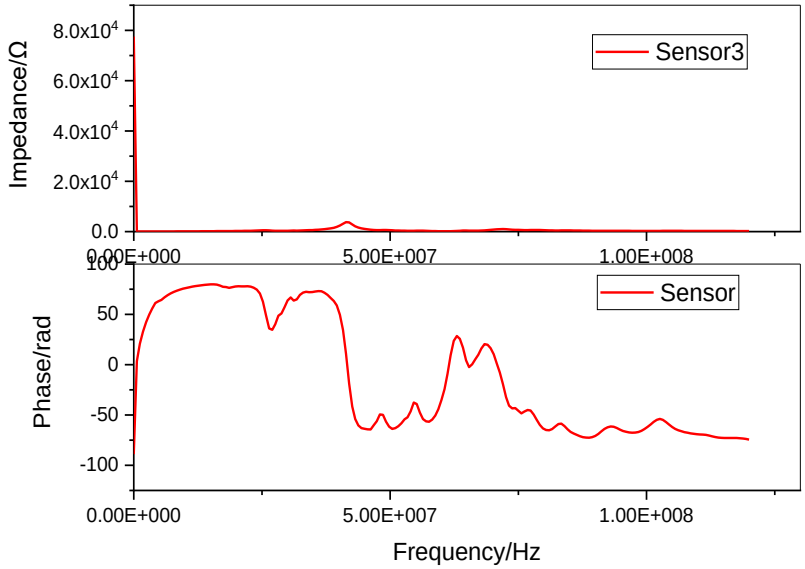

Figure 3.12: Frequency Response of Impedance of Bending Mode Sample

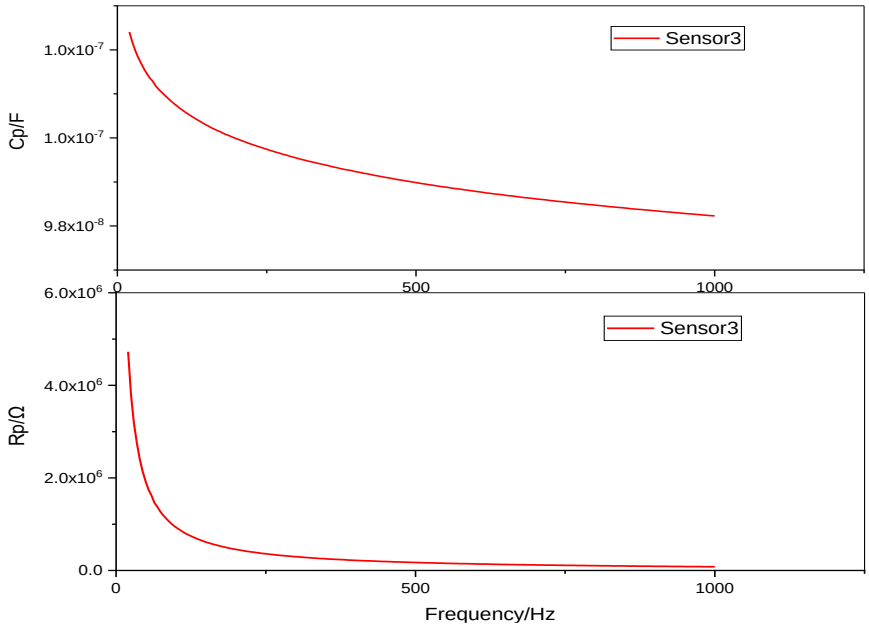

Figure 3.13: Equivalent Capacitance and Resistance of Bending Mode Sample

Table 3.1: Parameters of PZT sample

Parameters	Sensor Sample 1 (Compression)	Sensor sample 2 (Bending)
Rp (MΩ)	3.400	4.20
Cp (nF)	72.97	101.97
$d_{33}(\times 10^{-12} C/N)$	480	485
$-d_{31}(\times 10^{-12} C/N)$	240	242.5
E_{steel}(GPa)	210	210

According to Table 3.1, the average values for the equivalent capacitance and resistance of two compression mode sensor samples are 72.97 nF and 3.4 MΩ. As for bending mode, the values are 101.97 nF and 3.93 MΩ. Since the impedance of the sensor samples is huge, in order to idealize the sensor samples as an open loop, OP177 operation amplifier with an input resistance of 45 MΩ is chosen to build the interface circuit.

3.4 Experiment setup

This part mainly talks about the design and layout of the experiments to calibrate and compare these two different designs of sensors. The place chosen for the experimental installation is on the corridor of Benedum hall. A 27.5lb weight hand truck is used to simulate the vehicles. The floor is made of cement, which is rigid enough to support the sensor without affecting the experimental data.

As shown in Figure 3.14, the piezoelectric WIM sensor is fixed on the cement floor. The floor around the sensor is also padded with hard boards to ensure that the hand truck pass over the sensor smoothly. The width of the sensor beam is 5 cm (2 inches); the thickness is 1.27 cm (1/2 inches); the vector *v* points out the moving direction of the hand truck.

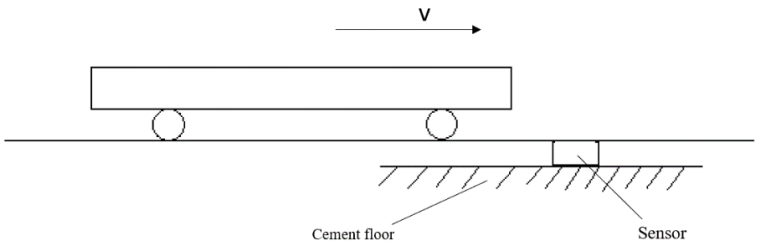

Figure 3.14: : Experimental sketch of the hand truck passing over the sensor

The hand truck will be pushed to have a certain initial speed and then released when approaching the sensor. Since the width of the sensor is 5cm, then we can use the stopwatch to measure the speed of the hand truck. The experiment is designed to measure three different weights at different speeds. Figure 3.15 illustrates the process and the layout of the experiment.

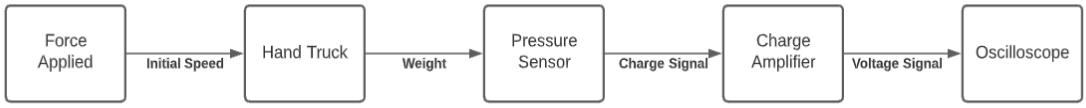

(a)

(b)

Figure 3.15: Illustration of the Experiment:(a) Flow chart ;(b) Experimental layout

3.4.1 Experimental Procedure and Results

The first step of the experiment is to set the charge amplifier to the desired time constant. Since the experiment is conducted in the corridor, the speed range of the hand truck is between 0.1m/s and 1m/s. Therefore, since the width of the sensor is 5cm, the low cutoff frequency of the sensor system should be lower than 2 Hz. Recall Table 3.1, the lower cutoff frequency of PZT sensor samples themselves without interface circuit is 0.64 Hz. However, its impedance is so large that the oscilloscope cannot measure the output voltage accurately. By setting the signal

conditioner elements as R_f=300 $k\Omega$, C_f=1μF, the system's low cutoff frequencies for compression mode sensors will be f_L=0.53 Hz. The impedance is lowered as well.

When the sensor is connected to the interface circuit, the output voltage is given by,

$$V_0 = -\frac{Q}{C_f} \ . \tag{3-27}$$

Since the value of Cf=1μF, which is about ten times larger than the Cp=72.97.7 nF, the output signal will be lowered by the charge amplifier. In order to get a strong enough signal, an operational amplifier is used to amplify the output signal.

For inverting operational amplifiers, the input impedance depends on the resistance R_i [26], and the input impedance should be larger than the output impedance of the source. The circuit is shown in Figure 29(b). Even though the charge amplifier lowered the output impedance of the PZT sensor, the resistance of R_i still needs to be very large to match the output impedance. The circuit is designed to amplify the input voltage ten times since the gain of inverting operational amplifier is calculated by,

$$G = -\frac{R_f}{R_i} \ , \tag{3-28}$$

The resistance of R_f needs to be 100 times larger than R_i. A large R_f brings a high output impedance, and the results will be affected if the circuit is connected to the oscilloscope. Therefore, the inverting op-amp is not applied in this experiment.

The advantage of the non-inverting operational amplifier (Figure 29(a)) is its high input impedance, which makes it suitable for conditioning high output impedance sources. The input impedance of the non-inverting amplifier equals the input resistance of the op-amp itself [27]. For OP177, the input resistance is 45 MΩ which is much larger than the output impedance of the sensor & charge amplifier system. The gain of the non-inverting op-amp is calculated by,

$$G = 1 + \frac{R_2}{R_1}\ , \tag{3-29}$$

By setting the amplifier element as $R_1 = 1k\Omega$ and $R_2 = 99k\Omega$, the gain of 100 can be achieved.

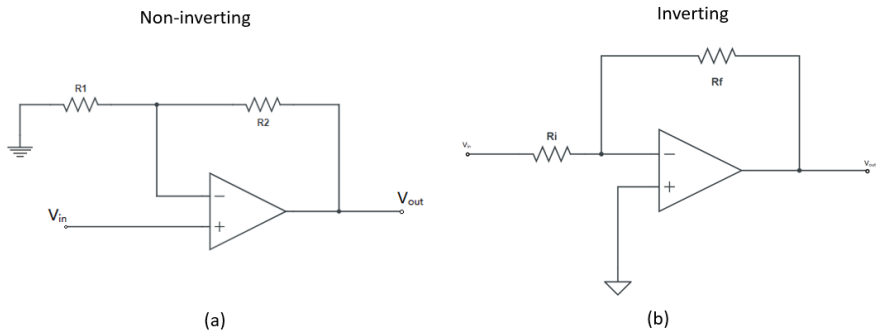

Figure 3.16: (a)Non-Inverting Op-Amp (b)Inverting Op-Amp

To investigate the relationship between the output voltage and applied load, three sets of experiments are conducted. Each set includes the time responses for the sensors when the hand trucks with the same weight roll over at two different speed. At the beginning of the experiment, the static weight of the front wheels of the hand truck is measured by weight scale and the static weight of each front wheel is 50N. Two 6kg boxes are used to change the loads. The loads will be placed on the front of the hand truck and the static weights of the wheels are measured before each set of experiments. The speed of the hand truck is measured by the stopwatch. The time responses for sensor 1, which measures the load of the right front wheel, are depict through Figure 3.17 to Figure 3.19. The maximum output voltages of each set of the experiment are given in Table 3.2. This table contains the loads and speeds of the hand truck for each set of the experiment as well.

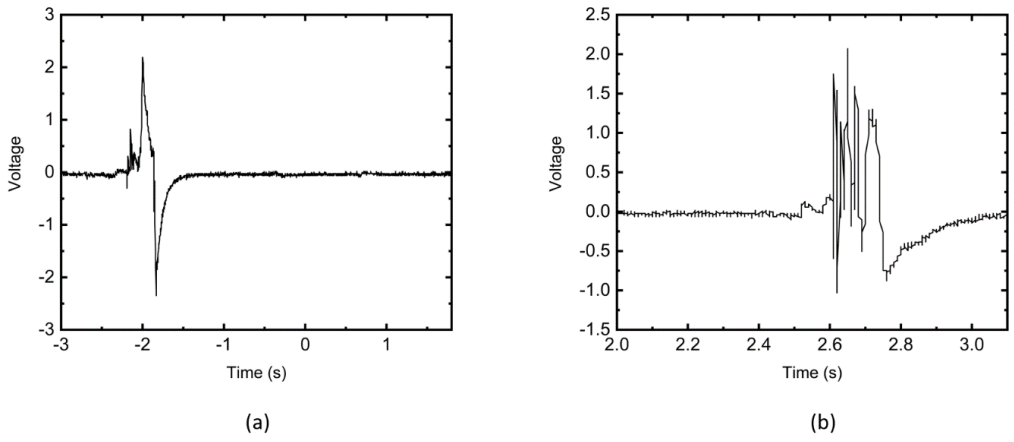

Figure 3.17: No Load

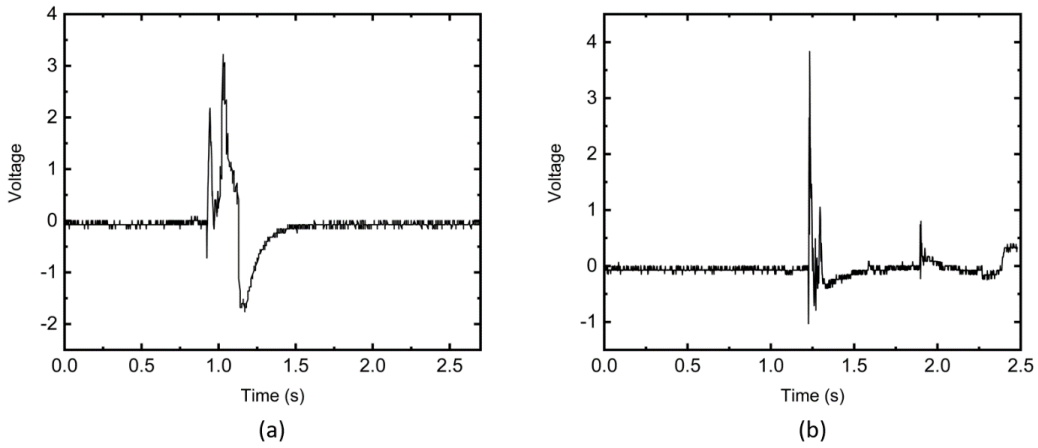

Figure 3.18: 1 Load

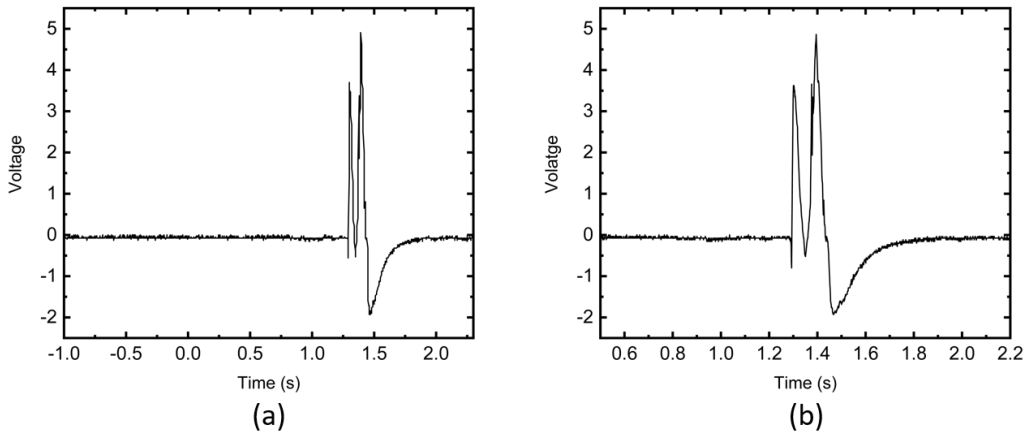

Figure 3.19: 2 Loads

Table 3.2: Output Voltage vs Load at Different Speed

Load/N	**Speed/ms^{-1}**	**Vmax/V**	**Speed/ms^{-1}**	**Vmax/V**
50	0.09	2.19	0.25	2.07
80	0.10	3.22	0.25	3.83
110	0.10	4.90	0.3	4.86

By observing the waveform through Figure 3.17 to Figure 3.19, it can be noticed that instead of a smooth waveform as our expectation, the waveform consists of multiple sharp peaks. Several reasons may result in this phenomenon. The first reason is that the pavement of the experiment is not smooth enough. The wheels may hit the sensor beams. These shocks display as the sharp peaks on the oscilloscope. The second possible reason is the vibration of the hand truck. Since a hand truck does not have a suspension system like a real car, the axles will vibrate when it moves.

According to Table 3.2, the relationship between the load and peak voltage is built. The results of the piezoelectric weigh-in-motion system for different vehicle speed is shown in Figure 3.20.

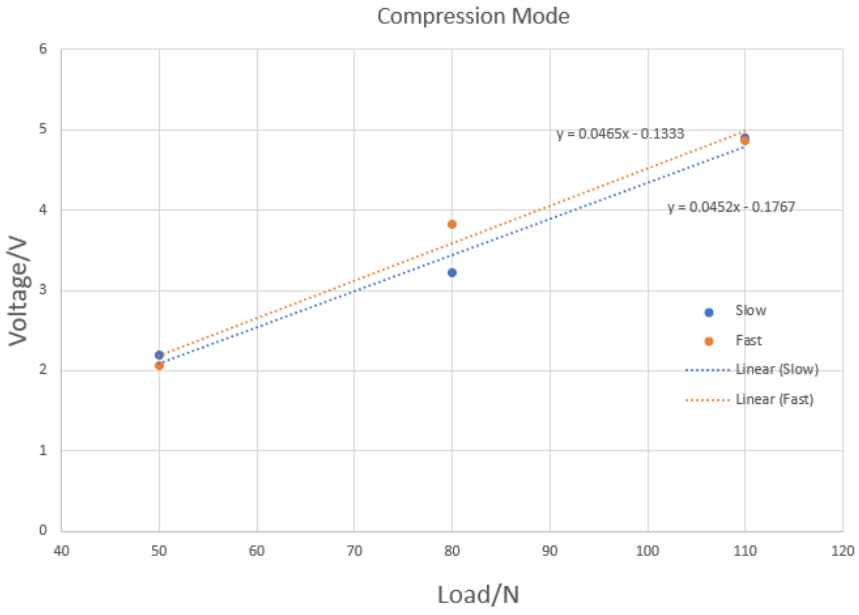

Figure 3.20: Calibration Curve

The voltage-load relationship in figure 33 is linearly fitted by least square approximation: V=0.0452*F-0.1767, V=0.0465*F-0.133 for slow speed and fast speed, respectively. The sensor sensitivity of the sensor is defined as the slope of the output characteristic curve. Therefore, the sensitivities of the piezoelectric WIM system for slow and fast vehicle speed are 45.2mV/N and 46.5mV/N, respectively. As for the theoretical value, since the piezoelectric sensor is connected to the interface circuit, the equation for calculating sensitivity is changed to,

$$Sensitivity = \frac{d_{33}}{C_f} \times G. \tag{3-30}$$

where d_{33}=450 pF/N, C_f = 1μF, and G=100. Therefore, the theoretical sensitivity is 50.0mV/N.

Table 3.3 Sensitivity of Compression Mode Sensor at Different Speeds

	Slow	Fast	Theoretical
Sensitivity(mV/N)	45.2	46.5	48

Then, the same experiment is conducted by the bending mode sensor design, and the results are shown through Figure 3.21 to 3.23, respectively. The maximum output voltages of each set of the experiment are given in Table 3.2. This table contains the loads and speeds of the hand truck for each set of the experiment.

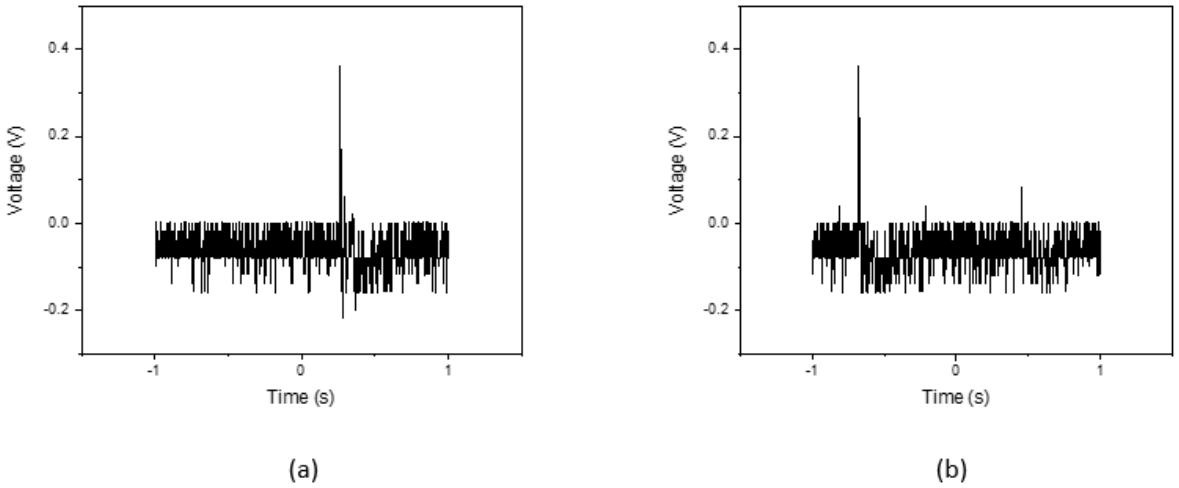

Figure 3.21: No Box

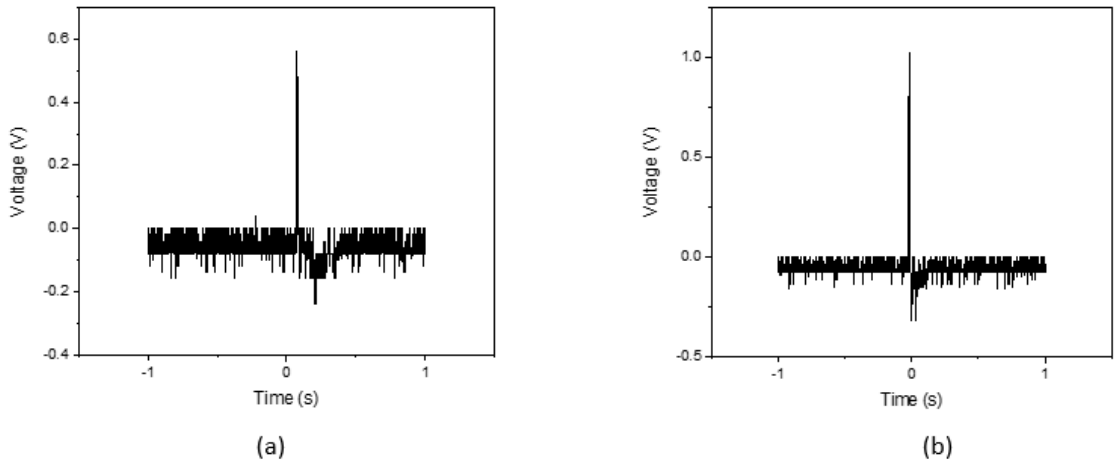

Figure 3.22: 1 Load

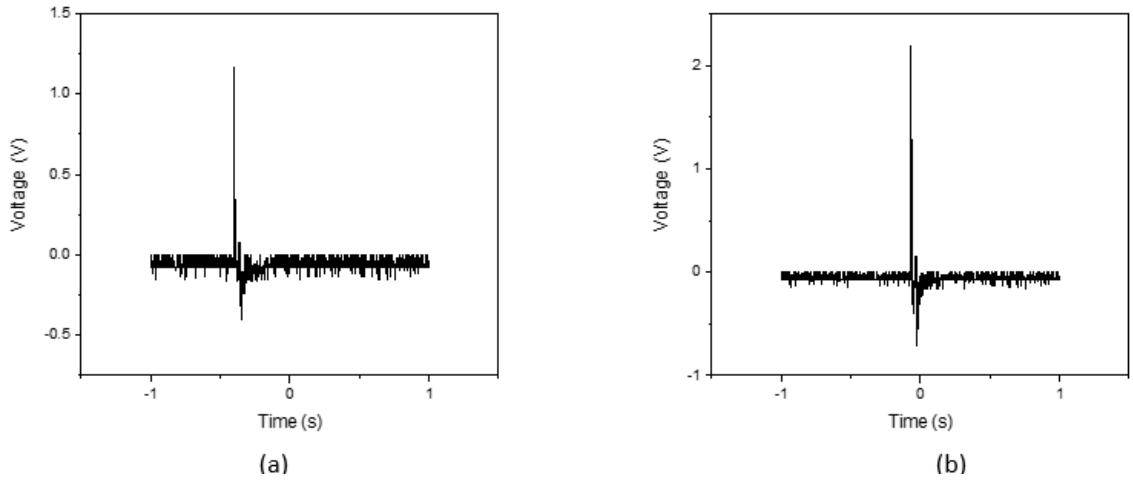

Figure 3.23: 2 Loads

Table 3.4: Output Voltage vs Load at Different Speed

Load/N	**Speed/ms^{-1}**	**Vmax/V**	**Speed/ms^{-1}**	**Vmax/V**
50	0.15	0.364	0.30	0.364
80	0.10	0.565	0.30	1.027
110	0.10	1.168	0.40	2.193

By observing the waveform through Figure 3.21 to Figure 3.23, it can be noticed that the output signal of the bending mode design is much smaller than the compression mode. Also, the speed of the vehicle has a significant influence on the results of the experiment. According to Table 3.4, the calibration curve for the bending mode sensor is built, which is shown in Figure 3.24.

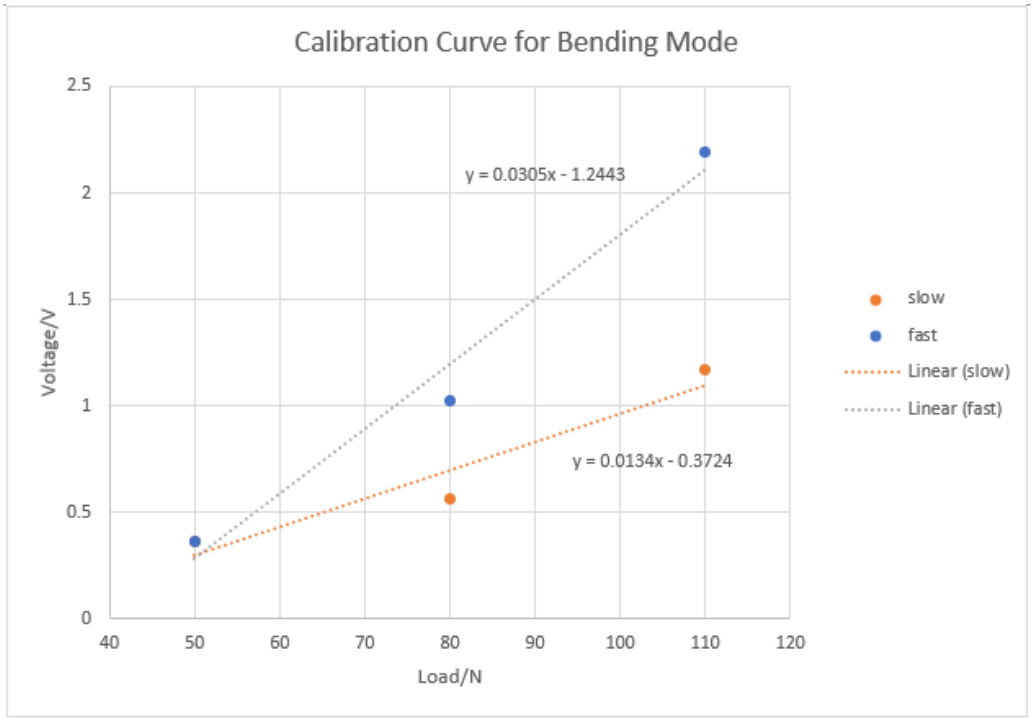

Figure 3.24: Calibration Curve of Bending Mode

The voltage-load relationship in Figure 3.24 is linearly fitted by least square approximation: V = 0.0134*F - 0.3724, V = 0.0305*F - 1.2443 for slow speed and fast speed, respectively. The sensitivities of the piezoelectric WIM system for slow and fast vehicle speed are 13.4mV/N and 30.5mV/N, respectively. As for the theoretical value, according to Equation 2.15, the theoretical value of the bending mode in this experiment is 33.6 mV/N.

3.4.2 Analysis of output signal in the frequency domain

After the experiment processes in the last chapter, the waveform of the output signal is acquired. In this part, the analysis of the waveform in the frequency domain is conducted. Fast

Fourier Transform is used to transfer the signal to the frequency domain. The FFT results of Figure 3.25 to Figure 3.27 are shown through Figure 3.21 to Figure 3.23, respectively.

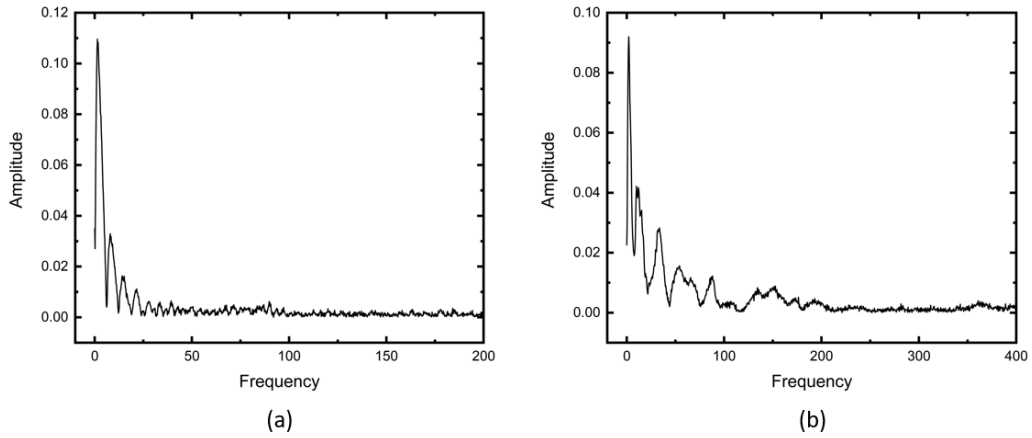

Figure 3.25: Frequency Spectrum of Figure 3.21

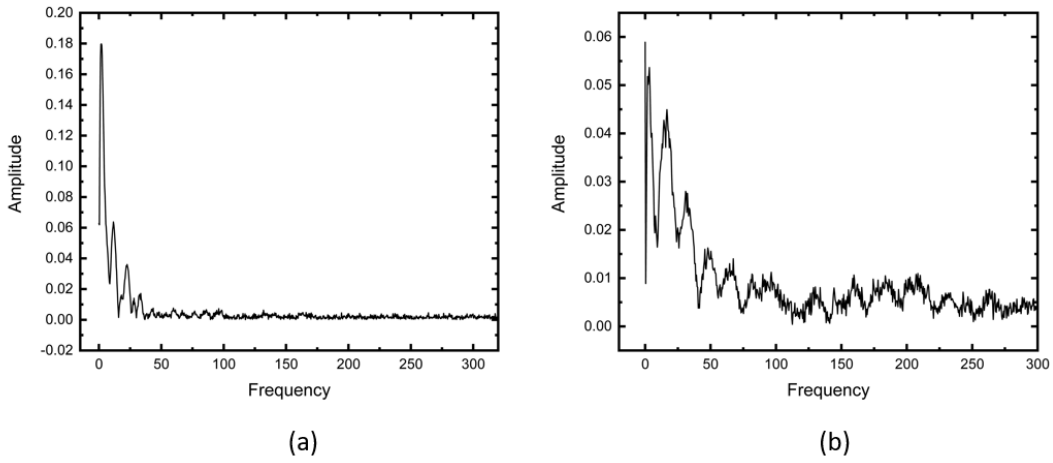

Figure 3.26: Frequency Spectrum of Figure 3.22

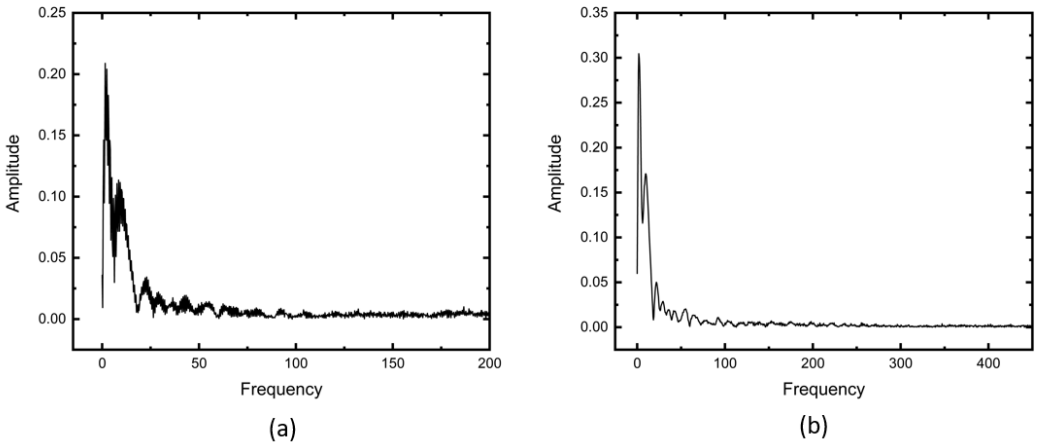

Figure 3.27: Frequency Spectrum of Figure 3.23

By observing the power spectrum, a frequency with the highest amplitude could be found, which could be considered as the frequency of the wave generated by the tire rolling over the sensing element. With the known width of the sensor W = 5 cm and the frequencies, it is possible to estimate the speed of the hand truck. The frequencies with the highest amplitude in these figures are listed in Table 3.4. This table includes the dominant frequencies of each experiment, the estimated speeds, and the speed measured by the stopwatch.

Table 3.4: Estimated Speed vs. Real Speed

Load/N	Dominant Frequency/Hz	Estimated Speed/ $cm \cdot s^{-1}$	Real Speed/ $cm \cdot s^{-1}$
50	1.4	7	9
50	2.5	12.5	25
80	1.87	9.35	10
80	3.04	15.2	25
110	1.94	9.7	10
110	3.33	16.65	30

3.4.3 Analysis and Discussion

The most important features for a system that is being used to convert mechanical energy into electrical energy like sensors are linearity and sensitivity. According to Figure 3.20, the compression mode piezoelectric WIM system performs good linearity of force-voltage relationship at both high speed and low speed. As for the sensitivity, the sensitivity at different speed conditions is almost the same. According to Table 3.3, comparing the experimental sensitivities with theoretical value, the sensitivity error is less than 10% for both high-speed and low-speed conditions. Two possible reasons result in the low sensitivity error.

The first reason is the simple structure of the compression mode piezoelectric sensor. Unlike other structural designs, the loads are directly applied to the sensing element of the compression mode sensor, which makes the energy loss is small. Therefore, the experimental sensitivity is close to the theoretical value.

The second reason is that the sample size of this experiment is too small. Due to the limitation of the experimental site and conditions, only 6 data points are analyzed. Also, d_{33} meter is not an accurate equipment, which will also cause the error. Even though the increasing trend of these data is reasonable, it is undeniable that the results may be inaccurate. Therefore, more samples with different loads and speeds should be tested in future work to support the results.

As for the bending mode design, according to Table 3.4 and Figure 3.24, the output signal is much lower than the compression mode design, and the sensitivity is highly affected by the speed of the hand truck. The sensitivities for both speeds are lower than the compression mode. The reason is that the sensitivity of the bending mode design depends on the shape of the beam. In this experiment, the beam is so thick that the deflection is too small, which results in a small output voltage. Therefore, bending mode is a better design for WIM system.

As for the estimation of speed by frequency domain analysis, in accordance with Table 3.4, we can find that the experimental values are inaccurate. The possible reason is that Fourier transform is used to analyze the periodic waveform. However, in this experiment, the signal is a pulse wave, which means that we cannot consider the dominant frequency as the frequency of the contact between the wheel and sensor ideally. However, recall Table 3.4, we can find that the dominant frequencies are proportional to the speeds. More experiments are needed in future work to figure out the relationship between the domination frequency and the vehicle speed.

4.0 Bluetooth Transmission Unit

In this part, a Bluetooth wireless signal transmission system is designed. In real life, it is impossible to build a traffic control center nearby every traffic sensor. Therefore, a wireless signal transmission system is needed for the traffic control center to monitor the road condition remotely.

4.1 Experimental Principle and Setup

4.1.1 Experimental Principle

In previous sections, the piezoelectric WIM system is designed to measure the weight of the vehicle. The piezoelectric sensor converts mechanical loads into voltage signals. In order to apply the voltage signals, a Bluetooth transmission unit based on Arduino Uno is designed in this experiment. The block diagram of the transmission unit is shown in figure 4.1.

The piezoelectric sensor generates the voltage signal, which is an analog signal. The voltage signal will be converted into a digital signal by the ADC (analog-to-digital converter) in the control circuit. ADC is a unit that converts an analog signal with a continuous-time and continuous-amplitude into a digital signal with discrete-time and amplitude. This process aims to transform the continuous analog signal into multiple binary numbers in the time domain. The binary numbers from a digital signal and the analog signal amplitude corresponding to the digital signal can be obtained by the ratio of the full-scale voltage range to the resolution. Then, the digital signal will be processed and operated by a microcontroller. Arduino Uno is used as the control

circuit because of its built-in analog-to-digital converter and multiple I/O modules, which matches the requirement of the experiment.

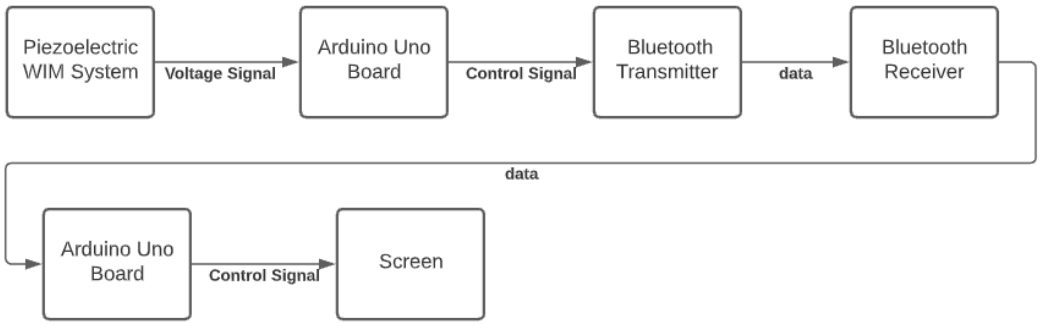

Figure 4.1:Flow Chart of the Transmission Unit

In this experiment, a two-way Bluetooth communication device is built to realize the wireless signal transmission. This device includes a master board and a slave board. The slave board is connected to the sensor and is responsible for collecting data and sending it to the master board via Bluetooth transmitter. The mater board is connected to the computer and displays the data. HC-05 Bluetooth transmitter is used in this experiment because it can both receive data and send data, which is required for a two-way communication device.

4.1.2 Experiment Setup

The sketch of slave and master board is shown in Figure 4.2 and Figure 4.3. For slave board, the piezoelectric sensor is connected to the analog port A_0. The V_{cc} and GND pins of the HC-05 Bluetooth module is connected to the 5V power supply and GND port, respectively. RxD (Receive Data) and TxD (Transmit Data) pins are connected to the TxD and RxD port of Arduino

respectively, the reason is that the Bluetooth transmitter needs to receive the processed data and send the Bluetooth communication data to Arduino. 9V DC battery is selected as the power supply.

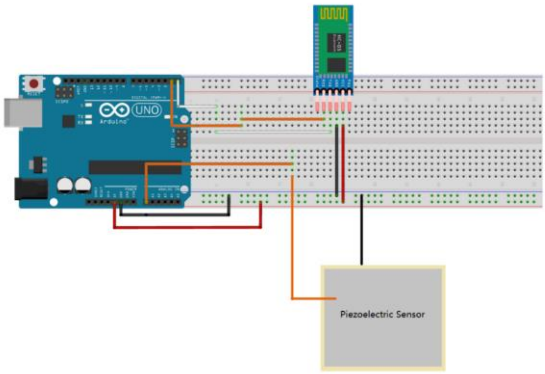

Figure 4.2: Sketch of Slave Board

As for the master board, the Arduino Uno board is connected to the computer to monitor the received data. The connection method of HC-05 Bluetooth module and Arduino Uno board is the same as the slave board.

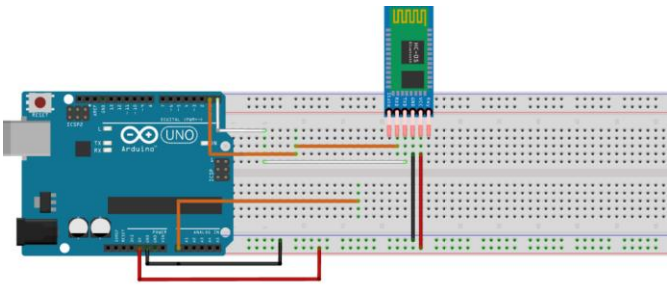

Figure 4.3: Sketch of Master Board

The Arduino programs for this experiment is attached in **Appendix A**.

4.2 Results and Analysis

The two-way communication system works successfully. The slave board prints the value of the loads on the screen of the computer every four seconds.

The program controls the slave board to collect the output data of the sensor, then uses bubble sort to find the maximum value of the sensor output. After that, since this value is a number from 0 to 1023, the program will multiply the number by 5/1024 to convert the digital signal to voltage. With the voltage and the calibration curve, the value of the load is yielded. Then, the EasyTransfer database will send this value to master board as a string via Bluetooth. As soon as the master board receive the data, it will be printed on the computer screen. The time constant of the piezoelectric sensor is 1.67s, as it is connected to the Arduino board, the time constant becomes longer due to the change in circuit, in order to ensure that the residual charge from the previous experiment will not affect the next time, a time delay with 4 seconds is set in the program.

For future work, a data logger will be designed. The voltage range of the analog port is 0-5V, which means that the negative value of voltage cannot be recorded. In this application, we only care about maximum output. However, if an analysis of the output waveform is needed, a data logger which can record the whole waveform is required.

5.0 Conclusions and Future Works

The main objectives include applying bending mode and compression mode design in piezoelectric weigh-in-motion systems and discussing the feasibility of estimating the vehicle speed by analyzing the signal in the frequency domain.

PZT ceramic plate is chosen as the sensing element of the sensor because of its large piezoelectric charge coefficient, moderate permittivity and high coupling factor, which makes the sensor more sensitive. The sensor structure is designed as compression mode and bending mode. For compression mode, a square PZT sensing element is placed under a steel beam. For bending mode, the sensing element is placed in the middle of a fixed-ended beam. The relations between output charge, voltage, and applied loads were derived theoretically. Since the sensor sensitivity is given by the ratio between the output voltage and input parameters, the theoretical sensitivity is also derived. By analyzing the piezoelectric element as a dynamic system, the effective range of a piezoelectric sensor can be derived. According to the theoretical derivation, a charge-amplifier circuit was designed to lower the output impedance and set the time constant to an expected value.

Compression mode and bending mode structure were compared. In the experiment, the hand truck with different weights is used to roll over the sensors. We also used a hand truck of the same weight to pass the sensor at different speeds in order to investigate the impact of the speed.

The results show that the compression mode performs good linearity under different mass and speeds. The experimental sensitivity of the compression mode is very close to the theoretical value since the simple structure takes low energy loss. As for bending mode, the experimental output voltage is much smaller than the compression mode, and it is highly affected by the speed of the hand truck. The reason is that we chose a thick beam to prevent the sensing element from

breaking since PZT is very fragile. However, the deflection of the thick beam is so small that the output signal is not strong enough. The experimental sensitivity is more closed to the theoretical value when the speed is higher. Therefore, compression mode design is a better design for Weigh-In-Motion system. Then, Fourier transform was used to get the frequency spectrum of the output signal. By observing the output signals, we found that its dominant frequency is related to the speeds. However, the estimated speeds, which is the product of the frequency and the width of sensing material, have huge error comparing with real value. In future work, more test needs to be conducted since the sample size in this experiment is too small due to the limitation of the experimental place.

In the final part, a Bluetooth wireless transmission system is built based on Arduino Uno was built. It consists of a slave board which collect and send the data to master board, and a mater board which receive and print the data on the screen. The system shows the loads of vehicles every four minutes. Due to the input voltage limitation of Arduino Uno, the transmission system is only able to display the maximum value of output signal. For future work, a data logger system is needed to be developed to record the whole waveform of the output signal.

Appendix A Arduino Code

Master Board

```
#include <EasyTransfer.h> //https://github.com/madsci1016/Arduino-EasyTransfer
struct Load_DATA_STRUCTURE
{
  float load ;
};
struct ACKNOWLEDGE
{
  boolean received = false;
};
Load_DATA_STRUCTURE data;       //define the received data structure
ACKNOWLEDGE acknowledge;        //define a confirmation signal
EasyTransfer ETin, ETout;
void setup() {
    pinMode(5, OUTPUT);
    Serial.begin(9600);
    ETin.begin(details(data), &Serial);
    ETout.begin(details(acknowledge), &Serial);
}

int loops = 0;

void loop() {

  if(ETin.receiveData()){
    String loadString = String(data.load,2);   //define the received load data as a string with
2 decimalplace
    Serial.print("Load = ");      //print the load value in serial monitor
    Serial.println(loadString);

    acknowledge.received = 1;
    ETout.sendData();    //send a received confirmation signal to slave board

    delay(10);
    acknowledge.received = 0;  //reset the confirmation signal
}
```

Slave board

```
const float g0 = 500, r = 100;
```

```
// these constants describe the pins. They won't change:
const int groundpin = 18;            // analog input pin 4 -- ground
const int powerpin = 19;             // analog input pin 5 -- voltage

struct SEND_DATA_STRUCTURE
{
  float pressure;
};

struct ACKNOWLEDGE
{
  boolean received = false;
};

SEND_DATA_STRUCTURE data;
ACKNOWLEDGE acknowledge;
EasyTransfer ETin, ETout; //We need two EasyTransfer object, one for the data we send, and one for the data we receive.

void setup() {
  Serial.begin(9600); //Baudrate of the Bluetooth modules
  ETout.begin(details(data), &Serial);
  ETin.begin(details(acknowledge), &Serial);
}

int counter = 0;
int loops = 0;
float abias, pbias;
float sensorVal, force;
float fMax = 0;

int fCount = 0;

void loop() {


   sensorVal=analogRead(A0);       //read data from the sensor

   data.load = fMax;

  if (counter == 0) //let the value measured in first 100ms out of 4s as bias to compensate the
  {
    fbias = sensorVal;
  }
```

```
    counter ++;

     if (sensorVal > fbias)
     {
       force = (sensorVal - fbias)*(5/1024)/(0.046);   //convert digital signal to load by multiplying 5/1024 and divided by the sensor sensitivity 0.046mV/N
        if (force < 3)
        {
         force = 0;
        }
       else
       {
        fCount ++;

       }
      }
      else
      {
       force = 0;
      }


      if (force > fMax)     //bubble sort to find the maximum value of load
       {
         fMax = force;
       }


   if (counter == 400)//Send data once every four seconds
   {
    ETout.sendData();
    counter = 0;
    fbias = 0;
    fMax = 0;
    fCount = 0;

   }

   delay(20);
   acknowledge.received = false;

  }
```

Bibliography

[1] A. A. Vives, *Piezoelectric transducers and applications*. Springer Berlin Heidelberg, 2008.

[2] S. J. Rupitsch, "Topics in Mining, Metallurgy and Materials Engineering Piezoelectric Sensors and Actuators Fundamentals and Applications." [Online]. Available: http://www.springer.com/series/11054.

[3] K. Uchino, "The development of piezoelectric materials and the new perspective."

[4] S. Katzir, "Who knew piezoelectricity? Rutherford and Langevin on submarine detection and the invention of sonar," *Notes and Records of the Royal Society*, vol. 66, no. 2. Royal Society, pp. 141–157, Jun. 20, 2012, doi: 10.1098/rsnr.2011.0049.

[5] W. A. Marrison, "The Evolution of the Quartz Crystal Clock," 1948. doi: 10.1002/j.1538-7305.1948.tb01343.x.

[6] "https://www.americanpiezo.com/piezo-theory/pzt.html." .

[7] Dincer I, "COMPREHENSIVE ENERGY SYSTEMS," 2018. [Online]. Available: http://ebookcentral.proquest.com/lib/pitt-ebooks/detail.action?docID=5313022.

[8] "'Sensor.' Merriam-Webster.com. Merriam-Webster, 2011. Web. 8 May 2011." .

[9] W. Gao, "Piezoelectric Pressure Sensors as Switching Devices," 2020.

[10] S. Kim, "LOW POWER ENERGY HARVESTING WITH PIEZOELECTRIC GENERATORS," 2002.

[11] W. Voigt, *Lehrbuch der Kristallphysik*. 1910.

[12] W. Zhang, C. Suo, and Q. Wang, “A novel sensor system for measuring wheel loads of vehicles on highways,” *Sensors*, vol. 8, no. 12, pp. 7671–7689, Dec. 2008, doi: 10.3390/s8127671.

[13] “https://www.fdot.gov/maintenance/weighstationlisting.shtm.”

[14] ASTM International, “Standard Practice for Classifying Highway Vehicles from Known Axle Count and Spacing.” [Online]. Available: www.astm.org.

[15] ASTM International, “Standard Specification for Highway Weigh-In-Motion (WIM) Systems with User Requirements and Test Methods,” 100 Barr Harbor Drive, PO Box C700, West Conshohocken, PA 19428-2959, United States. doi: 10.1520/E1318-09R17.

[16] S. Yuan, F. Ansari, X. Liu, and Y. Zhao, “Optic fiber-based dynamic pressure sensor for WIM system,” *Sensors and Actuators, A: Physical*, vol. 120, no. 1, pp. 53–58, Apr. 2005, doi: 10.1016/j.sna.2004.11.008.

[17] L. Cheng, H. Zhang, and Q. Li, “Design of a Capacitive Flexible Weighing Sensor for Vehicle WIM System,” *Sensors*, vol. 7, pp. 1530–1544, 2007, [Online]. Available: www.mdpi.org/sensors.

[18] “https://www.pcb.com/resources/technical-information/introduction-to-industrial-accelerometers.” .

[19] S. H. Choy, H. L. W. Chan, M. W. Ng, and P. C. K. Liu, “Study of 1-3 PZT fibre/epoxy composite force sensor,” *Applied Physics A: Materials Science and Processing*, vol. 81, no. 4, pp. 817–821, Sep. 2005, doi: 10.1007/s00339-004-2874-9.

[20] C. Mo, L. J. Radziemski, and W. W. Clark, “Analysis of piezoelectric circular diaphragm energy harvesters for use in a pressure fluctuating system,” *Smart Materials and Structures*, vol. 19, no. 2, 2010, doi: 10.1088/0964-1726/19/2/025016.

[21] M. A. Trindade and A. Benjeddou, “Effective electromechanical coupling coefficients of piezoelectric adaptive structures: Critical evaluation and optimization,” *Mechanics of Advanced Materials and Structures*, vol. 16, no. 3, pp. 210–223, Apr. 2009, doi: 10.1080/15376490902746863.

[22] A. K. Ramanathan, L. M. Headings, and M. J. Dapino, “Design optimization of flexible piezoelectric PVDF unimorphs for surface pressure transducer applications,” Mar. 2019, p. 6, doi: 10.1117/12.2514371.

[23] J. A. Svoboda and R. C. Dorf*, Introduction to electric circuits*. .

[24] Béla G. Lipták, *Instrument Engineers’ Handbook: Process control and optimization*, 4th Edition. 2003.

[25] “https://en.wikipedia.org/wiki/Piezoelectric_sensor.” .

[26] Texas Instruments, “Analog Engineer’s Circuit Cookbook: Amplifiers (Rev. A),” 2019.

[27] Texas Instruments, “AnalogEngineer’s Circuit:Amplifiers SBOA271A,” 2019. [Online]. Available: www.ti.com.